HOKKAIDO UNIVERSITY

Title	Comparison of ocean deoxygenation between CMIP models and observations in the North Pacific in the last half century
Author(s)	阿部, 佑美
Degree Grantor	北海道大学
Degree Name	博士(理学)
Dissertation Number	甲第16085号
Issue Date	2024-09-25
DOI	https://doi.org/10.14943/doctoral.k16085
Doc URL	https://hdl.handle.net/2115/93427
Type	doctoral thesis
File Information	Yumi_Abe.pdf

Hokkaido University Collection of Scholarly and Academic Papers : HUSCAP

Thesis for a Doctorate

博士学位論文

Comparison of ocean deoxygenation between CMIP models and observations in the North Pacific in the last half century

（北太平洋における過去半世紀の海洋貧酸素化に対する CMIP モデルと観測との比較）

Yumi Abe

阿部　佑美

Department of Natural History Sciences

Graduate School of Science

Hokkaido University

September 2024

Abstract

The amount of dissolved oxygen (O2) in the global ocean has been decreasing over the past half century. This phenomenon, called ocean deoxygenation, is one of the environmental problems associated with global warming that has attracted attention in recent years. It is important for the certainty of future predictions that the models adequately reproduce past O2 decreases. In Coupled Model Intercomparison Project (CMIP) Phase 5, the models underestimated the observations, which was problematic. In CMIP6, the model's O2 decrease falls within the variability of observations, but the comparison remains rough. Here we report the relationship between the observed and simulated O2 inventory changes in the North Pacific by analyzing observational data and the outputs of CMIP5 and 6 between 1958 and 2005 to understand the extent to which the CMIP models reproduce the observed O2 decrease. A total of 204 ensembles from 20 models were analyzed. Many of the models overestimate O2 climate values while some models show O2 decreases equal to or greater than observations. An inter-model empirical orthogonal function (EOF) analysis revealed that the different simulated magnitudes of the negative O2 trend is closely associated with the first EOF mode, and ensemble members with strong negative trends are characterized by large oxygen reduction in the subarctic North Pacific, especially around the boundaries between the North Pacific and the Sea of Okhotsk as well as the Bering Sea. The modeled strong O2 decrease in the subarctic North Pacific is consistent with the spatial pattern of the observed O2 trend. Further analysis of climate models indicated that the O2 decrease in the subarctic region was primarily caused by physical factors. This conclusion is supported by the significantly high correlation between the potential temperature and O2 inventory trend in the subarctic region, whereas an insignificant correlation coefficient is

present between dissolved organic carbon and the O2 inventory trend. However, the observations have a larger ratio of O2 inventory trend to temperature trend than any of the ensembles. Thus, the relationship between O2 and temperature change in the subarctic North Pacific seen in the CMIP5/6 simulations is not exact. Furthermore, we compared not only gridded data but also long-term observational data. At Station P, the models more significantly underestimated the trend and overestimated the climatological values compared to the observation. At 137°E, the observed O2 trend has decreased sharply in recent years, and the trend is outside the variability of the models. These detailed comparisons revealed that the CMIP models do not adequately reproduce the observed changes in O2 in the North Pacific.

Table of Contents

1 Introduction 4

2 Data and Methods 10

2.1 Model outputs 10
2.2 Observational data 13
2.3 Methods 14

3 Results 17

3.1 Oxygen inventory changes 17
3.2 Relationship between the oxygen inventory and spatial pattern 20
3.3 Environmental factors of oxygen decrease 22
3.4 Comparison of long-term observation data and CMIP models 26

4 Discussion and Conclusions 28

Acknowledgments 31

References 32

Table and Figures 47

1 Introduction

Oxygen, an important dissolved gas consumed by biological activities in the ocean, is saturated in the ocean surface layer by phytoplankton photosynthesis and gas exchange with the atmosphere. In processes such as photosynthesis and respiration, oxygen is directly linked to carbon dioxide. Consequently, understanding variation in dissolved oxygen (O2) is crucial for comprehending the carbon cycle, which is a significant issue in the context of global warming. In the past half century, the global O2 content has been decreasing due to global warming (IPCC, 2022). A rapid increase in surface water temperature leads to a decrease in the solubility of O2 in seawater, resulting in a lower saturated O2 concentration. Additionally, the increase in seawater temperature is larger and more rapid in the ocean surface layer than in the ocean interior. This strengthens ocean stratification and weakens ventilation and vertical mixing. Consequently, it becomes difficult for the saturated O2 in the ocean surface layer to be supplied to the ocean interior. This phenomenon of decreasing O2 levels in the ocean is called ocean deoxygenation. Ocean deoxygenation, along with global warming and acidification, impacts marine ecosystems on various scales (IPCC, 2013). For example, low O2 concentrations reduce growth, survival, and reproduction of individual fish (Townhill et al., 2017). Consequently, it poses a significant challenge to the use of marine systems by human society, including fisheries.

It is known that the Coupled Model Intercomparison Project (CMIP) models have been consistently underestimating past ocean deoxygenation (Oschlies et al., 2018). Recent estimates in observations indicate a global decline in O2 levels ranging from 0.5% to 3.3% in the surface to 1000 m layer compared to climatological averages for the period from 1970 to 2010 (Helm et al., 2011; Ito et al., 2017; Schmidtko et al., 2017; Bindoff et

al., 2019). In CMIP5 (Taylor et al., 2011), the models show a smaller O2 decrease than observed, particularly in the ocean interior during the period from 1960 to 2010 (Bopp et al., 2013; Cocco et al., 2013; Oschlies et al., 2018). The fact that CMIP models underestimate ocean deoxygenation is a significant concern, as it calls into question the reliability of future projections. The performance of biogeochemical models in CMIP6 (Eyring et al., 2016; O'Neill et al., 2016) has improved over CMIP5 due to the improved model resolution and the more complex representation of biogeochemical processes (Séférian et al., 2020; Ito et al., 2023). In CMIP6, the multi-model mean trend for the period from 1970 to 2010 at the depth of 100-600 m is included within the variability of observed trends between datasets (Kwiatkowski et al., 2020). However, it should be noted that their model-observation comparisons are limited, as they are only conducted for the depths of 100-600 m, where the variability among observational datasets is greatest, and only for the global ocean. Therefore, comparisons with observations, including CMIP6, remain inadequate, suggesting the need for further research to comprehend the relationship between observed and simulated O2 variations. It should be useful to compare observations and models in an ocean basin where data availability is relatively high and strong deoxygenation has been observed.

The North Pacific has experienced strong ocean deoxygenation, explaining approximately 18% of the global O2 decrease from 1960 to 2010 (Schmidtko et al., 2017). Compared with other regions of rapid deoxygenation, such as the South Atlantic and Southern Oceans, the North Pacific has better O2 data coverage (Ito et al. 2017). The observed O2 changes in the North Pacific are associated with cycles of internal variability (Andreev and Baturina, 2006; Sasano et al., 2018; Stramma et al., 2020) in addition to the effect of global warming. Moreover, O2 decreases in the northwestern North Pacific are

suggested to be attributed to a decrease in sea ice (Nakanowatari et al., 2007; Sasano et al., 2018). There are several long-term continuous hydrographic stations in the North Pacific. Ocean Weather Station P, located in the northeast Pacific (50°N, 145°W) (Freeland, 2007), is one of the longest available data on subsurface water properties, making it crucial for detecting climate change in the ocean. According to the data at Station P, O2 concentrations increased from the 1950s until the 1980s, after which they continued to decrease, with particularly large declines near the surface (Crawford and Peña, 2016; Ross et al., 2020; Whitney et al., 2007; Mecking et al., 2008). The 11.7% decrease in O2 from the surface to 4000 m from 1960 to 2018 is substantially greater than the global decrease trend of 2% (Cummins and Ross, 2020). In the western North Pacific, the Japan Meteorological Agency (JMA) conducts repeat observations along several longitudinal lines. One such line is at 137°E, where O2 data has been collected since 1967, indicating a decrease in O2 levels starting in the mid-1980s (Takatani et al., 2012; Oka et al., 2019). These observed O2 changes in the North Pacific are correlated with cycles of internal variability such as decadal oscillation or 18.6-year nodal tides (Yasuda et al., 2006; Osafune and Yasuda, 2006) in addition to the effect of global warming (Andreev and Baturina, 2006; Sasano et al., 2018; Stramma et al., 2020). Moreover, O2 decreases in the northwestern North Pacific are suggested to be attributed to a decrease in sea ice (Nakanowatari et al., 2007; Sasano et al., 2018).

The spatial pattern of the O2 trend in the CMIP5 multi-model mean is uniform compared with that of observations, and it does not reproduce the distribution and amplitude of the observed O2 trend (Stramma et al., 2012; Oschlies et al., 2017), although, for both global and North Pacific O2 concentrations, a high correlation exists between CMIP5/6 model outputs and observed climatology in subsurface waters (Takano et al.,

2018; Figure 4 in Séférian et al., 2020). It should be noted, however, that the CMIP model tends to overestimate climatological O2 in the North Pacific interior (Takano et al., 2018). A hindcast model experiment to simulate the effects of physical and biological factors on O2 changes in the North Pacific showed that O2 variability is dominated by ventilation and circulation, and that the effects of biological factors are limited to 30°N–40°N (Deutsch et al., 2006). Furthermore, a hindcast experiment conducted with the Community Earth System Model (CESM) experiment showed that O2 changes in the North Pacific are caused by internal variability linked changes in seawater temperatures that alter the depth of the isopycnal surface (Ito et al., 2019).

This study aims to determine whether the past O2 changes in the North Pacific where a large amount of observational data is available and strong ocean deoxygenation occurs, are consistent or not between observations and CMIP model ensemble members. Evaluating the performance of CMIP models can reveal their limitations and highlight important considerations for future projections. In discussing whether the CMIP model adequately reproduces observations, it is necessary to consider the influence of internal variability, as it is impossible for models to perfectly reproduce internal variability in the real world.

The advent of large ensemble members has made it possible to identify the uncertainty by internal variability as differences between ensemble members (Deser et al., 2014; Maher et al. 2021), as the initial conditions in climate simulations need only be perturbed slightly to rapidly vary climate conditions during specific periods. In climate simulations, the uncertainty is generally considered to arise from scenario uncertainty, model dependency, and internal variability (Hawkins and Sutton 2009). The separation of these uncertainties should be studied to assess future ocean deoxygenation (Frölicher

et al. 2016). Because we use only historical simulations, there is no scenario uncertainty, and thus only the internal variability and model dependency are the sources of uncertainty. A large ensemble analysis using CESM Large Ensemble experiment (Kay et al., 2014) was conducted for O2 (Long et al., 2016). The O2 decrease in the North Pacific occurs due to the combined effect of anthropogenic climate forcing and internal variability. CESM exhibits lower O2 concentrations than observed, suggesting an underestimation of internal variability and potentially weakening the response of anthropogenic forcing.

To determine whether the CMIP model can adequately reproduce the observations, including the effects of internal variability, we compare the observations with 204 ensembles of 20 CMIP5/6 models. Using nearly 200 ensemble members, including six models with more than 10 ensemble members, allows us to assess how well climate models capture the observed changes including internal variability, which has a significant effect on O2 changes in the North Pacific. Whether or not the observations are included in the ensemble members' variability is important in assessing the validity of the models. Additionally, comparisons were made with long-term observational data, including analyses of recent O2 decreases that were insufficiently captured by gridded data because of its data coverage.

The remainder of this paper is organized as follows. In Section 2, we describe the observational data and the CMIP model ensemble members used in this study. In Section 3, we first compare the O2 inventory changes in the North Pacific of the observations and those of the model ensemble members. Subsequently, the characteristics of a common spatial pattern among the model ensemble members are described. In Section 3, environmental factors related to the dominant spatial pattern among the model ensemble members are described. Finally, we compare the CMIP models with data from

long-term observation station. A discussion, including a summary of this study, is presented in Section 4.

2 Data and Methods

2.1 Model outputs

We analyze the outputs of 10 CMIP5 and CMIP6 models each, that is, 20 models in total, for their historical simulations (Table 1) to compare with a gridded observational dataset. The model outputs on the original grid shown in Table 1 are re-gridded to a common 1° × 1° grid in latitude and longitude using bilinear interpolation, and the vertical layers are interpolated to match the standard layers of World Ocean Atlas 2018 (WOA18) (0, 5, 10, 15, 20, 25, 30, 35, 40, 45, 50, 55, 60, 65, 70, 75, 80, 85, 90, 95, 100, 125, 150, 175, 200, 225, 250, 275, 300, 325, 350, 375, 400, 425, 450, 475, 500, 550, 600, 650, 700, 750, 800, 850, 900, 950, 1000 m from ocean sea surface). To determine whether artificial trends of substantial magnitudes occurred in historical simulations, the O2 inventory trends in the pre-industrial control (piControl) experiment (Eyring et al., 2016) were examined. We compared the O2 inventory trends from historical simulations with and without subtracting the piControl experiment's O2 concentration trend. There is little difference between the results of these two methods. Thus, in this study, trend subtraction from the piControl experiment is not conducted. We analyze ensemble members available for each model (Table 1) to assess the impact of internal variability on the O2 changes. That is, in CMIP terminology we use ensemble members “rxi1p1” from each CMIP5 model and “rxi1p1fx” from each CMIP6 model, where “rx” is realization (i.e. ensemble member), “i1” is initialization method, “p1” is physics, and “fx” is the recommended set of external forcings employed by the various modelling groups. The total ensemble number is 204, which is approximately one order of magnitude greater than the number of ensemble members used in previous studies of CMIP5/6 analyses (only the first ensemble member of each of the 23 models in Kwiatkowski et al., 2020).

For comparison with long-term observations, CMIP data were extended by connecting the outputs of the historical and future experiments, up to 2005 for CMIP5 and up to 2014 for CMIP6. For the scenarios, we selected the ones predicting the most severe global warming: RCP8.5 for CMIP5 and SSP5-8.5 for CMIP6. The number of ensemble members provided for future scenario outputs is smaller than those for historical experiments. In total, we used 111 model ensemble members for comparison with long-term observational data. For comparisons, we took the average of the surrounding four grid cells for the model data corresponding to one observation grid. For observations along a longitudinal line, the model data averaged the values from the longitude and the adjacent 0.5° lines.

To determine the extent of the influences of physical and biological factors on O2 changes in the CMIP model, we examine the potential temperature, sea ice volume, and dissolved organic carbon (DOC). The change in potential temperature due to global warming and internal variability is the primary driver of important physical changes for O2 changes. Specifically, because the solubility of O2 depends on water temperature, the saturated O2 concentration decreases as water temperature increases. In addition, because the increase in water temperature due to global warming is more rapid at the surface than in the ocean interior, leading to enhanced stratification, circulation-driven changes, and vertical migration of isopycnal surfaces. As the result, the O2-rich water masses in the surface layer are no longer supplied to the ocean interior. Another physical variable in this study is the sea ice volume, which is related to the formation of dense shelf water in the Okhotsk Sea which supplies O2-rich water to subsurface layers in the northwestern North Pacific. On the other hand, DOC is related to biological factors. O2 is consumed during the decomposition of organic matter by biological activity in the ocean interior. The total

organic carbon, which is the sum of DOC and particle organic carbon (POC), is used as an indicator of O2 consumption by biological activities (Doval and Hansell, 2000). However, the number of CMIP models that provide POC is very limited. Since DOC is the largest reservoir of reduced carbon in the ocean and its concentration in surface waters is about ten times that of POC, using DOC alone is sufficient as an indicator. In fact, the relationships between DOC and O2 utilization in the interior ocean have been widely studied (Carlson et al., 2010; Pan et al., 2014). Also, DOC is the variable with the most model outputs for variables related to three-dimensional organic carbon in the model ensemble members used in this study. Another indicator of O2 consumption by biological activity is export production, which expresses the amount of carbon sinking from the surface. Although this paper does not show export production results, similar findings were obtained as with DOC. The outputs of each variable are listed in Table 1.

For sea ice volume calculations, we use the same method as in Notz and SIMIP Community (2020). For the CMIP6 models, if a variable of sea ice volume is provided, *sivoln*, the short variable name in Earth System Grid Federation (https://aims2.llnl.gov/search/cmip6), is directly used; if it was not provided, we multiply a variable of sea ice volume per grid cell area, *sivol*, by the individual grid point area. If neither sea ice volume nor value per grid cell area is provided, we multiply the variables of sea ice concentration, *siconc*, sea ice thickness, *sithick*, and individual grid point area. For the CMIP5 models, only the variables of sea ice concentration and sea ice thickness are provided; thus, we multiply these variables and individual grid point areas. The trends in sea ice volume are calculated using the maximum sea ice volume between November and March in the following year.

2.2 Observational data

Gridded O2 concentration anomaly data produced by Ito et al. (2017) are used in this study on a 1° × 1° scale, with data from the surface to a depth of 1000 m, comprising 47 layers from 1950 to 2015 in annual intervals. The gridded anomaly data is generated using simple objective mapping with a Gaussian weight function, whose length scales are 1000 km and 500 km in the zonal and meridional directions, respectively. When calculating the O2 concentration trends for each grid, grids with fewer than 20 years of data is considered as missing values. Reflecting the changes in the observation numbers in World Ocean Database 2013 (WOD13), the temporal data coverage was relatively poor during the 1950s and 2010s. Thus, our analysis period is selected from 1958 to 2005, and our analysis domain is the North Pacific (15 °N–65 °N, 120 °E–100 °W).

Long-term observational data from Station P (50°N, 145°W) and the 137°E line were used, as these sites have particularly lengthy O2 observation periods. The Station P data used in this study are extracted from the entire archive of hydrographic data held at the Institute of Ocean Sciences (https://www.waterproperties.ca/mainlogin.php?refer=/data/, Accessed August 22, 2024) with O2 bottle and sensor data collected within 24 km of the nominal location of Station P. The vertical layers are interpolated to match the standard layers of WOA18 using Akima spline method (Akima, 1991). We must be cautious when calculating long-term trends at Station P, as temporal irregularities in data sampling have occurred due to the conclusion of the Canadian Weathership Program in 1981. To avoid the undue influence of data from the high frequency data sampling period prior to 1981 and the apparent trend associated with significant seasonal cycle aliasing in the surface mixed layer due to sampling three times per year after 1981, annual mean data with seasonal variations

removed are used in the trend calculations, as in Cummins and Ross (2020). Seasonal variations are estimated by simultaneously fitting the annual cycle and its semi-annual and quarterly harmonics, along with linear trends, to the monthly data. Seasonal variations are removed for the water masses above 150 dbar, and then the annual mean is calculated. We used data from the observation period 1957 to 2023 for our analysis. The data from the 137°E line was downloaded from the Japan Meteorological Agency's (JMA) website (https://www.data.jma.go.jp/kaiyou/db/mar_env/results/OI/137E_OI.html, Accessed August 22, 2024). Observations, which began in 1967, were conducted once each winter until 1972, and since then, they have been conducted twice a year, in both winter and summer. In this study, data from 15°N to 34°N were used, and the latitudinal interval was interpolated to 1°. The vertical layers are interpolated to match the standard layers of WOA18 using Akima spline method (Akima, 1991). We used data from the observation period 1967 to 2022 for our analysis.

In addition to the observational O2 data, we use temperature and salinity data to compare the simulated temperature changes with observations and calculate saturated oxygen concentrations. The data are obtained from the WOA18 (Locarinini et al., 2019; Zweng et al., 2019; Garcia et al., 2019), Met Hadley Centre's EN4.2 gridded data (Good et al., 2013), and the gridded data from JMA ver. 7.3.1 (Ishii et al., 2017). The outputs of all variables are re-gridded to a common 1° × 1° grid and interpolated to standard ocean depth. Because the WOA18 data are provided only for decadal climatologies on an average per 10 years from 1955 to 2004, the trend is calculated for this period. we use all available gridded data of temperature and salinity.

2.3 Methods

To estimate the observed O2 inventory in the North Pacific, we use a same

calculation method by Ito et al. (2017), using the following equation:

$$I_{O'_2}(t) = \left(\frac{V_{\mathrm{obs}}(t)}{V_{\mathrm{tot}}}\right)^{-1} \int O'_2(\boldsymbol{x}, t) dV,$$

where $I_{O'_2}(t)$ is the inventory of dissolved oxygen, $O'_2(x, t)$ is the anomaly of dissolved oxygen concentration, $\boldsymbol{x}$ is the position vector, t is the year, $V_{tot}$is the total volume of the ocean, and $V_{\mathrm{obs}}(t)$ is the total volume of the grid where oxygen data exist. Volume integration was performed for all grids where O2 data were available at each year. Then, considering that the number of O2 data grid cells differ annually, it is corrected by a coefficient, $\left(\frac{V_{\mathrm{obs}}(t)}{V_{\mathrm{tot}}}\right)^{-1}$. The total volume of the ocean is calculated using the water temperature data of WOD13.

In this study, six models (ACCESS-ESM1-5, CanESM5, IPSL-CM6A-LR, MIROC-ES2L, MPI-ESM1-2-HR, and MPI-ESM1-2-LR) with more than 10 ensemble members are considered as models with a large ensemble. The uncertainty of model dependency in the O2 inventory trend is expressed as the standard deviation among the ensemble means of each model. Furthermore, the uncertainty associated with internal variability is calculated by averaging the values of the standard deviations among the O2 inventory trends for ensemble members of each model. We use an empirical orthogonal function (EOF) analysis on the spatially distributed linear trend of O2 concentration at each horizontal grid point averaged from the surface to a depth of 1000 m across the 204 model ensemble members (known as the inter-model EOF analysis (Zhang et al. 2023; Zheng et al. 2016)) to determine representative variation patterns of O2 trend among ensemble members. We use this analysis because we hypothesize that the representative pattern differences across model ensemble members could be related to the varying magnitudes of O2 inventory trends and influencing mechanisms of the trends. By

extracting the dominant spatial pattern of O2 trends among model ensemble members through inter-model EOF analysis, it is possible to determine how spatial patterns of trends are related to inventory trends in the models and how they resemble observations. The inter-model EOF is calculated as follows: First, for each model ensemble member, the linear trend of O2 concentration is calculated at each horizontal grid point, averaged from the surface to depths of 1000 m as $Z(x,y,m)$, where x is the latitude, y is the longitude, and m is the number assigned to the model ensemble members (i.e., 1 to 204). The multi-model ensemble mean (MMEM), $\bar{Z}(x,y)$, across 204 ensemble members of the trend is subtracted from trends of respective ensemble members, yielding deviations in trends of respective ensemble members as, $Z'(x,y,m) = Z(x,y,m) - \bar{Z}(x,y)$. The inter-model EOF analysis expands the O2 trend deviation as follows:

$$Z'(x,y,m) = \sum_{n=1} X_n(x,y)M_n(m),$$

Where $X_n(x,y)$ is the spatial pattern of the n-th mode, and $M_n(m)$ is the model loading, which represents the amplitude of the spatial pattern for each model ensemble member.

3 Results

3.1 Oxygen inventory changes

First, we conduct a comparison to assess the consistency between the O2 climatology in the models and observation. As shown later, the subarctic region between 40°N and 65°N is the dominant region in the models for the overall O2 change in the North Pacific. Therefore, we present Figure 1, which shows the vertical distribution of climatological O2 concentration averaged in the latitudinal band between 40°N and 65 °N. At depths greater than 200 m, most models have higher O2 concentration climatology than observation, and the difference with observation increases as the depth increases until around 700 m depth, where the decrease in observed O2 climatology levels off. This inconsistency between the climatologies of models and observations was shown in previous studies (Cabré et al., 2015; Takano et al., 2018; Takano et al., 2023) and should be considered when comparing the modeled O2 inventory trend with observations, because models may not well reproduce background field associated with O2 concentration.

The observed and simulated time series of O2 anomaly inventories in the North Pacific are shown in Figure 2. The observed O2 inventory generally increased until approximately 1990, followed by large negative anomalies in the late 1990s and the early 2000s. An increase in the O2 inventory in the early period is also found in previous global observational analyses (Garcia et al. 2005; Ito et al. 2017). The record-low O2 concentrations occurred in the Oyashio area during the late 1990s (Sasano et al. 2018), which are also observed at Station P in the early 2000s (Whitney et al. 2007). This variation remained unchanged when the depth at which the inventory was calculated was varied. The simulated O2 inventories show large diversity in their temporal evolution.

The multi-model ensemble mean increases until the mid-1980s and later decreased; however, each ensemble member exhibits substantial differences. IPSL-CM5B-LR and MPI-ESM-1-2-HAM generally increase, whereas CESM1-BGC, MPI-ESM-LR and MPI-ESM-MR generally decrease. Almost all other models increase in earlier decades and subsequently decreased. Regardless of the diversity of simulated O2 inventories, no ensemble member shows large negative anomalies in the late 1990s and the early 2000s, as observed.

To evaluate how representative model skill in the North Pacific is for the global ocean, we examine the relationship between the regional and global difference in the observed and model O2 inventory trend. The relationship is obtained by (i) the difference between the O2 inventory trend of each model ensemble member and the observed O2 inventory trend is calculated for both the North Pacific and global ocean, and then (ii) computing the correlation coefficient between the North Pacific and the global ocean. We find a correlation coefficient of 0.535, which is statistically significant. Thus, if the modeled O2 inventory trend is close to the observation in the North Pacific, the modeled O2 inventory trend is also close to the observation in global ocean. However, it must be noted that the share of total O2 observations in the North Pacific is about 10% greater than the North Pacific's share of the global ocean area.

Figure 3 shows the spatial patterns of the trends of the vertically averaged O2 concentrations in the observations and MMEM values. The observed trend is characterized by a strong decrease in the subarctic North Pacific, including the northwest North Pacific, especially around the Kuril Islands, between the Sea of Okhotsk and the North Pacific; around the Bering Sea; in the Gulf of Alaska; and offshore California, consistent with previous regional observational studies for the northwest North Pacific

(Nakanowatari et al., 2007) and offshore California (Pierce et al., 2012; Crauford and Peña, 2016). However, the spatial pattern of the MMEM trend displays more uniformity than the observed trend.

Figure 4 shows the linear trends of the O2 inventory anomaly from 1958 to 2005 in the observation and models. The observed trend of -3.68×10^{12} mol/yr is thrice as large as the MMEM trend (-1.06×10^{12} mol/yr). The confidence interval for the observed O2 trend is -5.40×10^{12} - -1.75×10^{12} mol/yr, thus the MMEM trend is outside this range. Although the observed trend is higher than the simulated trend, it is included in the variability of the simulation. Nineteen model ensemble members out of 204 ensemble members (i.e., 9.3%) have larger than observed negative O2 trends. Figure 4 also suggested that internal variability plays an important role in the uncertainty of the modeled O2 trend, as displayed by the positive and negative trends for different ensembles (HadGEM2-ES, IPSL-CM5A-MR, MPI-ESM-LR, MPI-ESM1-2-HR, ACCESS-ESM1-5, CanESM5, IPSL-CM6A-LR, MIROC-ES2L, MPI-ESM1-2-HR, MPI-ESM1-2-LR, and NorESM2-MM). To assess the impact of internal variability on the variability of O2 inventory trends across model ensemble members, we calculate the uncertainty of model dependency and internal variability. We obtain the uncertainty of model dependency calculated as the inter-model standard deviation of the large ensemble mean in each model is 9.36×10^{11} mol/yr and internal variability calculated as inter-model mean of the standard deviation of the large ensemble in each model is 1.72×10^{12} mol/yr, respectively. The uncertainty in the O2 inventory trend due to internal variability is larger than the uncertainty due to model dependency, affecting the differences in O2 inventory trends among the models. However, as previously mentioned, it is important to consider

that many models have higher climatological values than observations. In particular, IPSL-CM6A-LR and MPI-ESM1-2-LR include the observed trends within the ensemble member variability, but the large difference in climatology between these models and observations from Figure 1 suggests that the models do not correctly reproduce the background filed, and that O2 may not be decreasing for the same reasons as observed.

3.2 Relationship between the oxygen inventory and spatial pattern

In contrast to the spatially uniform MMEM trend (Figure 3b), the model ensemble members generally show spatial variability in the O2 concentration trends. Figure 5 shows the standard deviation of the O2 concentration trend averaged from the surface to 1000 m. The variability of the trend is particularly large in the western subarctic, the Bering Sea, and especially the Sea of Okhotsk. The locations with the greatest variation among these model ensemble members are, as noted above, those with the largest negative trends in the spatial pattern of trends in the observations shown in Figure 3 (a).

To investigate whether there is a relationship between the inter-model variability in the spatial pattern of O2 trends and inter-model variability in O2 inventory trends in the North Pacific shown in Figure 4, we examine the spatial patterns of vertically averaged O2 trends for model ensemble members with large negative O2 inventory trends and those with large positive O2 inventory trends. We specifically compare the ensemble member with the largest negative trends and the ensemble member with the largest positive trends within the top four models (ACCESS-ESM1-5, IPSL-CM6A-LR, MPI-ESM1-2-HR, and MPI-ESM1-2-LR) characterized by the highest variability in O2 inventory trends within each model shown in Figure 4. From Figure 6, it is evident that ensemble members with large negative O2 inventory trends show strong negative trends

in the subarctic region, the Sea of Okhotsk, and the Bering Sea. On the other hand, ensemble members with large positive O2 inventory trends show a corresponding distribution of positive trends in those regions. In IPSL-CM6A-LR, the negative trend in the Sea of Okhotsk is large in the ensemble member showing a positive trend in O2 inventory. Looking at each depth level in detail, although the negative trend is large in all depth level in the Sea of Okhotsk, the positive trend is largely distributed in the subarctic region at depths of 300 m and deeper. While the vertically averaged trend diminishes the pronounced positive trend, it is likely that this ensemble member demonstrates a positive trend in the O2 inventory trend due to the substantial positive trend in the subarctic region at deeper depths as in other models. Therefore, it is suggested that the differences in trends in the subarctic region, the Sea of Okhotsk, and the Bering Sea also affect the differences in O2 inventory trends.

To extract the representative spatial patterns of the vertically averaged O2 concentration trend, inter-model EOF analysis is applied as explained in Section 2. The explained variance of the first mode was 0.28, which is much higher than that of the second mode (0.10). Figure 7 (a) and (b) show the model loadings and spatial pattern, respectively, for the first EOF mode. As the spatial pattern indicates strong negative amplitudes in the subarctic North Pacific, especially in the western part and Sea of Okhotsk, ensemble members with positive loadings imply that their negative O2 trend in this region is larger than that of the MMEM. Therefore, it is expected that a higher loading would result in a more pronounced negative trend, indicating a potential correlation between the loadings and the O2 inventory trend.

Figure 8 (a) shows a scatter plot of the loadings of the first EOF mode shown in Figure 7 (a) and the O2 inventory trends in Figure 4. The correlation coefficient between

them is significant at -0.87 ($p<0.01$); thus, this relationship accounts for approximately two-thirds of the variance of the O2 inventory trends among ensemble members. Therefore, ensemble members with the largest, positive loadings on the first EOF mode have a stronger negative trend in O2 inventories. Since the largest negative amplitudes of the first EOF occur in the subarctic North Pacific, the strong negative relationship between the loadings and the simulated trend in the O2 inventories suggests that these simulated trends are mainly driven by inter-model variability in the subarctic North Pacific.

To ascertain whether the factors that result in the spatial pattern of the first EOF mode are consistent with the factors that reduce dissolved oxygen in the observation, it is important to investigate whether model ensemble members with positively high loading have a spatial pattern like the observations. Therefore, we analyze the relationship between the EOF loadings and the similarity in the spatial pattern of the O2 trend in the North Pacific between the ensemble members and observation, using spatial correlation coefficients in vertically averaged O2 concentration trends between the observation and each ensemble member as a measure of similarity (Figure 8b). The correlation coefficient between the EOF loadings and the spatial correlation coefficients is 0.77 ($p<0.01$); therefore, the spatial patterns of the model ensemble members with high loadings are like those observed in association with strong O2 reduction in the subarctic North Pacific. An ensemble member that has a strong negative trend in this region, indicating a closer resemblance to the observed trend pattern, tends to exhibit a stronger decrease in O2 throughout the basin.

3.3 Environmental factors of oxygen decrease

The results of the previous subsections indicate the importance of O2 changes in

the subarctic North Pacific in observations and simulations. To determine why O2 trend variability between models is greater in the North Pacific subarctic, and whether it is consistent with observed O2 trend variability, this section discusses environmental factors that can influence O2 variation in that region. We first examine the oxygen saturation (O2sat) and apparent oxygen utilization (AOU). Here, O2sat is calculated according to the equation by Garcia and Gordon (1992), using temperature and salinity data. Temperature and salinity data are obtained from EN4, data from JMA, and WOA18. The AOU is calculated as AOU=O2sat-O2, where the O2 value from observations is estimated by adding the climatological O2 concentration from WOA18 to the O2 anomaly from Ito et al. (2017). We used the WOA18 annually averaged climatology from 1960 to 2017. To determine the extent to which the O2 inventory trend is explained by the AOU inventory trend and the O2sat inventory trend, we calculate the ratio of the AOU and O2sat inventory trends to the O2 inventory trend, respectively. The AOU inventory trends dominate the observed O2 and simulated inventory trends in the subarctic North Pacific. The AOU inventory trend accounts for approximately 100% of the observed O2 inventory trend. To examine the contributions of O2sat and AOU to ensemble member differences, we use multiple regression analysis to obtain partial regression coefficients for O2sat and AOU inventory trends related to O2 inventory trend in the subarctic North Pacific. The partial regression coefficient of the O2sat inventory trend on the O2 inventory trend is 0.0096, and that of the AOU inventory trend against the O2 inventory trend is -0.98. Thus, the O2 inventory trend in the subarctic North Pacific is dominated by the AOU inventory trend in the model ensemble members.

Next, we examine the influence of the physical and biological environmental

factors, that is, ocean temperature, sea ice, and DOC, on the O2 inventory trends in the subarctic North Pacific. Subarctic inventory trends are calculated for temperature and DOC at each grid point and averaged in the subarctic North Pacific from the surface to depths of 1000 m, between 40°N and 65°N. For sea ice, the inventory trend of the sea ice volume is calculated by horizontal integration of sea ice volume at each grid point. We did not use salinity in our analysis because a multiple regression analysis with inter-model AOU trend in the subarctic North Pacific as the dependent variable and water temperature, salinity, and DOC trend as explanatory variables showed that the partial regression coefficients for water temperature and DOC were statistically significant, whereas the partial regression coefficient for salinity was very small. This indicates that the contribution of salinity to O2 changes in the subarctic region can be ignored.

The correlations between these variables and subarctic O2 inventory trends are used to determine their relationship with the O2 change in the subarctic North Pacific. Figure 9 shows the relationship between the subarctic O2 inventory and the trend for each environmental factor. The potential temperature had a correlation of -0.24 ($p<0.01$), and temperature in the subsurface layer (200-600 m) has a higher correlation with O2 (-0.35) than that in the surface layer (-0.12). The sea ice volume had a moderate correlation of 0.19 ($p=0.011$). The correlation coefficient between the temperature trends and sea-ice trends is -0.62 ($p<0.01$). The correlation coefficient with DOC is small and insignificant, even at the 10% significance level. The observed O2 inventory trend in the subarctic North Pacific is higher than that in most of the ensemble members, while 68.5% of the total 204 ensemble members show a stronger positive temperature trend than observed. This suggests that the model does not adequately reproduce the O2 decrease in response

to the physical processes changes that occur as water temperature increases.

Figure 9 (a) shows that the correlation between potential temperature and O2 inventory trend is not strong. However, the regression map between the O2 inventory and the potential temperature trend in the North Pacific shown in Figure 10 indicates that potential temperature changes in the western subarctic region and the Sea of Okhotsk are strongly related to the O2 inventory trend. In fact, the correlation coefficient between potential temperature around the Sea of Okhotsk (45° to 65°N, 140° to 160°E) and the North Pacific O2 inventory trend was highly correlated at -0.55. For SST, the relationship with the North Pacific O2 inventory trend has the same spatial pattern as in Figure 10. This spatial pattern is not entirely consistent with the PDO spatial pattern consisting of the SST anomaly which is one sign in the central and western North Pacific and the opposite sign along the eastern North Pacific (Mantua et al., 1997).

These results show that the modeled O2 inventory trends in the subarctic North Pacific are explained by temperature trends, which are partly related to sea ice, suggesting that changes in ocean circulation associated with changes in water temperature are important for the O2 decrease in the subarctic North Pacific. The importance of changes in circulation has been revealed by observational analysis (Nakanowatari et al., 2007), then the models is consistent with observations. Also, the small influence of biological factors in the subarctic North Pacific is consistent with the results of a previous study (Deutch et al., 2006). However, the observed O2 inventory trend in the subarctic North Pacific is higher than that in most of the ensembles, whereas the observed temperature trends are weaker than those in most simulations (Figure 9a). Consequently, the observed ratios of the O2 inventory trend relative to the temperature trend, that is, the O2 inventory trend divided by the temperature trend, are greater than in any of the ensembles with a

negative O2 trend and a positive temperature trend. Therefore, the relationship between O2 and temperature change in the subarctic North Pacific found in the CMIP5 and CMIP6 simulations is inaccurate with nature, which requires further investigation.

3.4 Comparison of long-term observation data and CMIP models

We have compared CMIP models with gridded observation data. However, according to Table 5.2 in Bindoff et al. (2019), three global gridded datasets show considerable differences due to different gridding methods. Therefore, we further evaluate the reproducibility of CMIP models by comparing them with long-term observational data, which are closer to raw data.

Figure 11 shows the trends of vertically integrated O2 concentration at Station P from the surface to 1000 m for observation and each CMIP model ensemble member. Two models in CMIP5 (HadGEM2-CC, HadGEM2-ES) and two models in CMIP6 (ACCESS-ESM1-5, CanESM5) have ensemble members with larger decrease trends than observations, while all other models show smaller decrease trends in all their ensemble members. Among the four models with ensemble members showing larger decrease trends than observations, only one ensemble member from each shows a larger decrease trend than observed, except for ACCESS-ESM1-5. Thus, more significantly than across the North Pacific, the CMIP models underestimate the decrease in O2 at Station P compared to observation.

The time-averaged vertically integrated O2 concentration is larger in all model ensembles except for two in CMIP5 (GFDL-ESM2G, MPI-ESM-MR), compared to observation (Figure 12). Although the ACCESS-ESM1-5 shows a decrease trend consistent with observations, its time-averaged O2 concentration is approximately 50 mol/m² higher than observed, raising questions about the reproducibility of the

background field. Therefore, the underestimation of O2 trends and the overestimation of O2 climatological values by CMIP models, as revealed by comparisons with gridded data, are also evident at Station P. This further strengthens the conclusion that there is a significant discrepancy between the models and observations in the subarctic region.

Next, we examine the relationship between the CMIP models and observational data along the 137°E, which is located in the subtropical region. Figure 13 shows the time series of the area-averaged observational data from the surface to 1000 m depth along the 137°E line between 15°N and 34°N. In both winter and summer, O2 concentrations have been rapidly decreasing since the late 2010s. However, such a recent rapid O2 decrease does not appear in the CMIP models (Figure 14).

Figure 15 (a) shows the trend in annual mean O2 concentration for observations from 1972 to 2022. The decreasing trend is large south of 27°N from 300 m to 800 m. This decreasing trend is consistently large in both winter and summer. To determine if the observed trend is within the variability of the CMIP model trends, Figure 15 (b) shows where the observed trend lies within the range of CMIP model trends. Near the surface and below 600 m depth, the observed decrease trends are outside the range of the model trends at almost all latitudes. Furthermore, in the grids where the observed decrease trends are particularly large, the observed trends are outside the range of model trend variability. Therefore, it is evident that O2 levels have been rapidly decreasing along the 137°E line in recent years and the model ensemble members do not capture the observed trends.

4 Discussion and Conclusions

We investigate O2 changes in the North Pacific from 1958 to 2005 using a gridded observational dataset and 204 ensemble members of CMIP5/6 historical simulations. The results of the EOF analysis indicate that the importance of the O2 decrease in the Sea of Okhotsk and subarctic region for the O2 decrease in the North Pacific is consistent with the observations. The observed negative trend for O2 inventory in the North Pacific is thrice higher than the MMEM trend. Although some models with ensemble members exhibit a larger negative trend than observed, as indicated by Figures 1 and 4, these models have climatologies that are inconsistent with observations. This raises doubts about the fidelity of the underlying physical and biogeochemical models, casting doubt on whether the modeled O2 decline reproduce the observed O2 decline for consistent physics with nature. The subarctic North Pacific and Sea of Okhotsk are vital regions (Figure 6, 7b) that explains most of the observed O2 inventory trend magnitude (Figures 4, 8). These regions dominantly provide the major differences among ensemble members, as found in the EOF analysis (Figure 7a) The ensemble members having higher negative O2 trends in this region also have strong basin-wide negative O2 trends (Figure 8). This accompanies a higher similarity to the negative O2 trend of observations (Figure 3a). Among the examined environmental factors, that is, water temperature, sea ice volume, and DOC, water temperature is the most strongly related to the ensemble member differences of the simulated O2 inventory trends in the subarctic North Pacific, followed by sea ice volume, whereas DOC is not significantly correlated. The simulated temperature-oxygen relation, however, is not in line with the observed relationship, that is, the observed O2 inventory trend in the subarctic North Pacific divided by temperature change is stronger than in any of the 204 ensembles. The comparison between long-term

observational data from Station P and CMIP models shows similar characteristics across the North Pacific. The observed decrease trend is larger than in most models, while the climatological inventory values in most CMIP models are overestimated compared to observations (Figures 11, 12). From the data along the 137°E line, it is indicated that observed O2 has been rapidly decreasing in recent years (Figure 13). Consequently, in the subtropical region, the observed trends are no longer within the variability of the model trends (Figure 15b).

The discrepancy between CMIP models and observations of ocean deoxygenation have already been suggested by global analysis (Oschlies et al., 2018). In this study, we confirmed in more detail that CMIP models show inconsistencies with observed O2 decreases in the North Pacific, which is a relatively well-observed region among areas exhibiting strong ocean deoxygenation, such as the South Atlantic and the Southern Ocean (Schmidtko et al., 2017) based on the comparison of O2 climatology and inventory trends in multi-ensemble members and their ratio to water temperature trends. In addition, the use of long-term observational data addresses the limitations of gridded data, making the results more robust.

Our results raise concerns about future climatic model projections. We have showed that the models do not accurately reproduce the mechanisms of O2 decrease, such as underestimating the O2 reduction in response to rising water temperatures. Therefore, it is highly likely that future O2 decreases is represented by different factors than those in reality. In addition, it is important for future projections that the model accurately reproduces climate values. Figure 8 in Cabre et al. (2015) shows the climatologies for WOA09 and CMIP5, and the difference between historical experiments and future projections for CMIP5. The models have significantly larger climatology than

observations, especially in the high latitudes of the North Pacific. In this region, most models predict a future decrease of 15 mmol/m^3 or more compared to the historical experiment, but this decrease is too large compared to the observed climatology.

Currently, the discrepancy between models and observations is considered to be an issue for both physical and biogeochemical models. In terms of trends, the observed spatial patterns and EOF analysis results indicate that O2 decrease in marginal seas such as the Sea of Okhotsk and the Bering Sea is important. The contribution of these seas to biological production in the North Pacific is also shown by Nishioka et al. (2020). However, CMIP models face issues such as insufficient vertical mixing at straits (Tatebe et al., 2019) and the inability to adequately separate marginal seas from the open ocean. The inconsistency between observations and models at Station P can be attributed to these circulation issues. This is because the O2 decrease at Station P is considered to be due to O2 decrease in North Pacific Intermediate Water formed in the Sea of Okhotsk (Cummins and Ross, 2022). In terms of climatology, it is necessary to improve the parameterization of biogeochemical models. The vertical distribution of potential density in the subarctic North Pacific does not differ between observations and models (Figure 16), suggesting that the models can reproduce the water masses in this region. However, according to Cabré et al. (2015), CMIP models tend to have sinking carbon from the surface reaching deeper depths than in reality, which prevents O2 from being consumed at shallower depths, resulting in higher climatology compared to observations.

Acknowledgments

I would like to express my sincere gratitude to my supervisor, Prof. Shoshiro Minobe, for his tremendous support and many valuable suggestions and discussions throughout this study. Thanks to his attentive and meticulous guidance, I was able to complete this thesis. I would also like to extend my heartfelt thanks to my Ph.D. committee members, Profs: Masaru Inatsu, Yoshinori Sasaki, Yousuke Sato, and Shinya Kouketsu, for taking the time to review my thesis despite their busy schedules. Finally, I wish to express my deep appreciation to my parents, Hiroshi and Masumi, and my beloved husband, Keita, for their unwavering support.

References

Akima, H. (1991). A method of univariate interpolation that has the accuracy of a third-degree polynomial. *ACM Transactions on Mathematical Software*, 17(3), 344-366. doi: 10.1145/114697.116810

Andreev, A. G., and Baturina, V. I. (2006). Impacts of tides and atmospheric forcing variability on dissolved oxygen in the subarctic North Pacific. *Journal of Geophysical Research: Oceans*, 111(7). doi: 10.1029/2005JC003103

Bindoff, N. L., Cheung, W. W. L., Kairo, J. G., Arístegui, J., Guinder, V. A., Hallberg, R., Hilmi, N., Jiao, N., Karim, M. S., Levin, L., O'Donoghue, A., Purca Cuicapusa, S. R., Rinkevich, B., Suga, T., Tagliabue, A., and Williamson P. (2019). Changing ocean, marine ecosystems, and dependent communities. *In: IPCC Special Report on the Ocean and Cryosphere in a Changing Climate* [Pörtner, H. -O., Roberts, D. C., Masson-Delmotte, V., Zhai, P., Tignor, M., Poloczanska, E., Mintenbeck, K., Alegría, A., Nicolai, M., Okem, A., Petzold, J., Rama, B., Weyer, N. M. (eds.)]. Cambridge University Press, Cambridge, pp. 447–587. doi: 10.1017/9781009157964.007

Bopp, L., le Quéré, C., Heimann, M., Manning, A. C., and Monfray, P. (2002). Climate-induced oceanic oxygen fluxes: Implications for the contemporary carbon budget. *Global Biogeochemical Cycles*, 16(2), 6-1-6–13. doi: 10.1029/2001gb001445

Boucher, O., Servonnat, J., Albright, A. L., Aumont, O., Balkanski, Y., Bastrikov, V., Bekki, S., Bonnet, R., Bony, S., Bopp, L., Braconnot, P., Brockmann, P., Cadule, P., Caubel, A., Cheruy, F., Codron, F., Cozic, A., Cugnet, D., D'Andrea, F., Davini, P., de Lavergne, C., Denvil, S., Deshayes, J., Devilliers, M., Ducharne, A., Dufresne, J. -L., Dupont, E., Éthé, C., Fairhead, L., Falletti, L., Flavoni, S., Foujols, M. -A., Gardoll, S., Gastineau, G., Ghattas, J., Grandpeix, J. -Y., Guenet, B., Guez, L. E.,

Guilyardi, E., Guimberteau, M., Hauglustaine, D., Hourdin, F., Idelkadi, A., Joussaume, S., Kageyama, M., Khodri, M., Krinner, G., Lebas, N., Levavasseur, G., Lévy, C., Li, L., lott, F., Lurton, T., Luyssaert, S., Madec, G., Madeleine, J. -B., Maignan, F., Marchand, M., Marti, O., Mellul, L., Meurdesoif, Y., Mignot, J., Musat, I., Ottlé, C., Peylin, P., Planton, Y., Polcher, J., Rio, C., Rochetin, N., Rousset, C., Sepulchre, P., Sima, A., Swingedouw, D., Thiéblemont, R., Traore, A. K., Vancoppenolle, M., Vial, J., Vialard, J., Viovy, N., and Vuichard, N. (2020). Presentation and Evaluation of the IPSL-CM6A-LR Climate Model. *Journal of Advances in Modeling Earth Systems*, 12(7). doi: 10.1029/2019MS002010

Carlson, C. A., Hansell, D. A., Nelson, N. B., Siegel, D. A., Smethie, W. M., Khatiwala, S., Meyers, M. M., and Halewood, E. (2010). Dissolved organic carbon export and subsequent remineralization in the mesopelagic and bathypelagic realms of the North Atlantic basin. *Deep-Sea Research Part II: Topical Studies in Oceanography*, 57(16), 1433–1445. doi: 10.1016/j.dsr2.2010.02.013

Collins, W. J., Bellouin, N., Doutriaux-Boucher, M., Gedney, N., Halloran, P., Hinton, T., Hughes, J., Jones, C. D., Joshi, M., Liddicoat, S., Martin, G., O'Connor, F., Rae, J., Senior, C., Sitch, S., Totterdell, I., Wiltshire, A., and Woodward, S. (2011). Development and evaluation of an Earth-System model - HadGEM2. *Geoscientific Model Development*, 4(4), 1051–1075. doi: 10.5194/gmd-4-1051-2011

Crawford, W. R., and Peña, M. A. (2016). Decadal trends in oxygen concentration in subsurface waters of the Northeast Pacific Ocean. *Atmosphere - Ocean*, 54(2), 171–192. doi: 10.1080/07055900.2016.1158145

Cummins, P. F., and Ross, T. (2020). Secular trends in water properties at station P in the northeast Pacific: an updated analysis. *Progress in Oceanography*, 186 (2020),

p.102329. doi: 10.1016/j.pocean.2020.102329

Deser, C., Phillips, A. S., Alexander, M. A., and Smoliak, B. V. (2014). Projecting North American Climate over the Next 50 Years: Uncertainty due to Internal Variability. *Journal of Climate*, 27(6), 2271-2296. doi: 10.1175/JCLI-D-13-00451.1

Deutsch, C., Emerson, S., and Thompson, L. A. (2006). Physical-biological interactions in North Pacific oxygen variability. *Journal of Geophysical Research: Oceans*, 111(9). doi: 10.1029/2005JC003179

Doval, M. D., and Hansell, D. A. (2000). Organic carbon and apparent oxygen utilization in the western South Pacific and the central Indian Oceans. *Marine Chemistry*, 68(3), 249-264. doi: 10.1016/S0304-4203(99)00081-X

Dufresne, J. L., Foujols, M. A., Denvil, S., Caubel, A., Marti, O., Aumont, O., Balkanski, Y., Bekki, S., Bellenger, H., Benshila, R., Bony, S., Bopp, L., Braconnot, P., Brockmann, P., Cadule, P., Cheruy, F., Codron, F., Cozic, A., Cugnet, D., de Noblet, N., Duvel, J. -P., Ethé, C., Fairhead, L., Fichefet, T., Flavoni, S., Friedlingstein, P., Grandpeix, J. -Y., Guez, L., Guilyardi, E., Hauglustaine, D., Hourdin, F., Idelkadi, A., Ghattas, J., Joussaume, S., Kageyama, M., Krinner, G., Labetoulle, S., Lahellec, A., Lefebvre, M. -P., Lefevre, F., Levy, C., Li, Z. X., Lloyd, J., Lott, F., Madec, G., Mancip, M., Marchand, M., Masson, S., Meurdesoif, Y., Mignot, J., Musat, I., Parouty, S., Polcher, J., Rio, C., Schulz, M., Swingedouw, D., Szopa, S., Talandier, C., Terray, P., Viovy, P., and Vuichard, N. (2013). Climate change projections using the IPSL-CM5 Earth System Model: From CMIP3 to CMIP5. *Climate Dynamics*, 40(9–10), 2123–2165. doi: 10.1007/s00382-012-1636-1

Dunne, J. P., Bociu, I., Bronselaer, B., Guo, H., John, J. G., Krasting, J. P., Stock, C. A., Winton, M., and Zadeh, N. (2020). Simple global ocean Biogeochemistry with Light,

Iron, Nutrients and Gas version 2 (BLINGv2): Model description and simulation characteristics in GFDL's CM4.0. *Journal of Advances in Modeling Earth Systems*, 12, e2019MS002008. doi: 10.1029/2019MS002008

Dunne, J. P., John, J. G., Shevliakova, S., Stouffer, R. J., Krasting, J. P., Malyshev, S. L., Milly, P. C. D., Sentman, L. T., Adcroft, A. J., Cooke, W., Dunne, K. A., Griffies, S. M., Hallberg, R. W., Harrison, M. J., Levy, H., Wittenberg, A. T., Phillips, P. J., and Zadeh, N. (2013). GFDL's ESM2 global coupled climate-carbon earth system models. Part II: Carbon system formulation and baseline simulation characteristics. *Journal of Climate*, 26(7), 2247–2267. doi: 10.1175/JCLI-D-12-00150.1

Eyring, V., Bony, S., Meehl, G. A., Senior, C. A., Stevens, B., Stouffer, R. J., and Taylor, K. E. (2016). Overview of the Coupled Model Intercomparison Project Phase 6 (CMIP6) experimental design and organization. *Geoscientific Model Development*, 9, 1937–1958. doi: 10.5194/gmd-9-1937-2016.

Freeland, H. J. (2007). A short history of Ocean Station Papa and Line P. *Progress in Oceanography*, 75, 253–265. doi: 10.1016/j.pocean.2007.08.005.

Frölicher, T. L., Joos, F., Plattner, G. K., Steinacher, M., and Doney, S. C. (2009). Natural variability and anthropogenic trends in oceanic oxygen in a coupled carbon cycle-climate model ensemble. *Global Biogeochemical Cycles*, 23(1). doi: 10.1029/2008GB003316

Garcia, H. E., Boyer, T. P., Levitus, S., Locarnini, R. A., and Antonov, J. (2005). On the variability of dissolved oxygen and apparent oxygen utilization content for the upper world ocean: 1955 to 1998. *Geophysical Research Letters*, 32(9), 1–4. doi: 10.1029/2004GL022286

Garcia, H. E., and Gordon, L. (1992). Oxygen solubility in seawater: Better fitting

equations. *Limnol. And Oceanogr*., 37, 1307–1312. doi: 10.4319/lo.1992.37.6.1307

Garcia H. E., Weathers, K. W., Paver, C. R., Smolyar, I., Boyer, T. P., Locarnini, R. A., Zweng, M. M., Mishonov, A. V., Baranova, O. K., Seidov, D., and Reagan, J. R. (2019). World Ocean Atlas 2018, Volume 3: Dissolved Oxygen, Apparent Oxygen Utilization, and Dissolved Oxygen Saturation. A. Mishonov Technical Editor. *NOAA Atlas NESDIS* 83, 38pp.

Gent, P. R. (2011). The Gent-McWilliams parameterization: 20/20 hindsight. *Ocean Modelling*, 39(1–2), 2–9. doi: 10.1016/j.ocemod.2010.08.002

Giorgetta, M. A., Jungclaus, J., Reick, C. H., Legutke, S., Bader, J., Böttinger, M., Brovkin, V., Crueger, T., Esch, M., Fieg, K., Glushak, K., Gayler, V., Haak, H., Hollweg, H.-D., Ilyina, T., Kinne, S., Kornblueh, L., Matei, D., Mauritsen, T., Mikolajewicz, U., Mueller, W., Notz, D., Pithan, F., Raddatz, T., Rast, S., Redler, R., Roeckner, E., Schmidt, H., Schnur, R., Segschneider, J., Six, K. D., Stockhause, M., Timmreck, C., Wegner, J., Widmann, H., Wieners, K. -H., Claussen, M., Marotzke, J., and Stevens, B. (2013). Climate and carbon cycle changes from 1850 to 2100 in MPI-ESM simulations for the Coupled Model Intercomparison Project phase 5. *Journal of Advances in Modeling Earth Systems*, 5(3), 572–597. doi: 10.1002/jame.20038

Good, S. A., Martin, M. J., and Rayner, N. A. (2013). EN4: Quality controlled ocean temperature and salinity profiles and monthly objective analyses with uncertainty estimates. *Journal of Geophysical Research: Oceans*, 118(12), 6704–6716. doi: 10.1002/2013JC009067

Grégoire, M., Garçon, V., Garcia, H., Breitburg, D., Isensee, K., Oschlies, A., Telszewski, M., Barth, A., Bittig, H. C., Carstensen, J., Carval, T., Chai, F., Chavez, F., Conley,

D., Coppola, L., Crowe, S., Currie, K., Dai, M., Deflandre, B., Dewitte, B., Diaz, R., Garcia-Robledo, E., Gilbert, D., Giorgetti, A., Glud, R., Gutierrez, D., Hosoda, S., Ishii, M., Jacinto, G., Langdon, C., Lauvset, S. K., Levin, L. A., Limburg, K. E., Mehrtens, H., Montes, I., Naqvi, W., Paulmier, A., Pfeil, B., Pitcher, G., Pouliquen, S., Rabalais, N., Rabouille, C., Recape, V., Roman, M., Rose, K., Rudnick, D., Rummer, J., Schmechtig, C., Schmidtko, S., Seibel, B., Slomp, C., Sumalia, U. R., Tanhua, T., Thierry, V., Uchida, H., Wanninkhof, R., and Yasuhara, M. (2021). A Global Ocean Oxygen Database and Atlas for Assessing and Predicting Deoxygenation and Ocean Health in the Open and Coastal Ocean. *Frontiers in Marine Science,* 8, 724913. doi: 10.3389/fmars.2021.724913

Hajima, T., Watanabe, M., Yamamoto, A., Tatebe, H., Noguchi, M. A., Abe, M., Ohgaito, R., Ito, A., Yamazaki, D., Okajima, H., Ito, A., Takata, K., Ogochi, K., Watanabe, S., and Kawamiya, M. (2020). Development of the MIROC-ES2L Earth system model and the evaluation of biogeochemical processes and feedbacks. *Geoscientific Model Development*, 13(5), 2197–2244. doi: 10.5194/gmd-13-2197-2020

Hawkins, E., and Sutton, R. (2009). The potential to narrow uncertainty in regional climate predictions. *Bulletin of the American Meteorological Society*, 90(8), 1095–1107. doi: 10.1175/2009BAMS2607.1

Helm, K. P., Bindoff, N. L., and Church, J. A. (2011). Observed decreases in oxygen content of the global ocean. *Geophysical Research Letters*, 38(23), 1–6. doi: 10.1029/2011GL049513

IPCC. (2013). Climate Change 2013: The Physical Science Basis. *Contribution of Working Group I to the Fifth Assessment Report of the Intergovernmental Panel on Climate Change* [Stocker, T. F., Qin, D., Plattner, G. -K., Tignor, M., Allen, S. K.,

Boschung, J., Nauels, A., Xia, Y., Bex V., and Midgley, P. M. (eds.)]. *Cambridge University Press, Cambridge*, 1535 pp.

IPCC. (2022). Changing Ocean, Marine Ecosystems, and Dependent Communities. In C. Intergovernmental Panel on Climate (Ed.), *The Ocean and Cryosphere in a Changing Climate: Special Report of the Intergovernmental Panel on Climate Change* (pp. 447-588). *Cambridge: Cambridge University Press.*

Ishii, M., Fukuda, Y., Hirahara, S., Yasui, S., Suzuki, T., and Sato, K. (2017). Accuracy of Global Upper Ocean Heat Content Estimation Expected from Present Observational Data Sets. *SOLA*, 13(0), 163–167. doi: 10.2151/sola.2017-030

Ito, T., Minobe, S., Long, M. C., and Deutsch, C. (2017). Upper ocean O2 trends: 1958–2015. *Geophysical Research Letters*, 44(9), 4214–4223. doi: 10.1002/2017GL073613

Ito, T., Long, M. C., Deutsch, C., Minobe, S., and Sun, D. (2019). Mechanisms of Low-Frequency Oxygen Variability in the North Pacific. *Global Biogeochemical Cycles*, 33(2), 110–124. doi: 10.1029/2018GB005987

Ito, T., Garcia, H. E., Wang, Z., Minobe, S., Long, M. C., Cebrian, J., Reagan, J., Boyer, T., Paver, C., Bouchard, C., Takano, Y., Cervania, A., and Deutsch, C. A. (2023). Underestimation of global O2 loss in optimally interpolated historical ocean observations. *Biogeosciences Discussions,* 2023, 1–22. doi: 10.5194/bg-2023-72

Kay, J. E., Deser, C., Phillips, A., Mai, A., Hannay, C., Strand, G., Arblaster, J. M., Bates, S. C., Danabasoglu, G., Edwards, J., Holland, M., Kushner, P., Lamarque, J. F., Lawrence, D., Lindsay, K., Middleton, A., Munoz, E., Neale, R., Oleson, K., Polvani, L., and Vertenstein, M. (2015). The community earth system model (CESM) large ensemble project: A community resource for studying climate change in the presence

of internal climate variability. *Bulletin of the American Meteorological Society*, 96(8), 1333–1349. doi: 10.1175/BAMS-D-13-00255.1

Keeling, R. F., and Garcia, H. E. (2002). The change in oceanic O2 inventory associated with recent global warming. *Proceedings of the National Academy of Sciences of the United States of America*, 99(12), 7848–7853. doi: 10.1073/pnas.122154899

Kwiatkowski, L., Torres, O., Bopp, L., Aumont, O., Chamberlain, M., Christian, J., Dunne, J., Gehlen, M., Ilyina, T., John, J., Lenton, A., Li, H., Lovenduski, N., Orr, J., Palmieri, J., Schwinger, J., Séférian, R., Stock, C., Tagliabue, A., Takano, Y., Tjiputra, J., Toyama, K., Tsujino, H., Watanabe, M., Yamamoto, A., Yool, A., and Ziehn, T. (2020). Twenty-first century ocean warming, acidification, deoxygenation, and upper ocean nutrient decline from CMIP6 model projections. *Biogeosciences Discussions*, 1–43. doi: 10.5194/bg-2020-16

Locarnini, R. A., Mishonov, A. V., Baranova, O. K., Boyer, T. P., Zweng, M. M., Garcia, H. E., Reagan, J. R., Seidov, D., Weathers, K. W., Paver, C. R., and Smolyar, I. V. (2019). World Ocean Atlas 2018, Volume 1: Temperature. A. Mishonov, Technical Editor. *NOAA Atlas NESDIS* 81, 52pp.

Long, M. C., Deutsch, C., and Ito, T. (2016). Finding forced trends in oceanic oxygen. *Global Biogeochemical Cycles*, 30(2), 381–397. doi: 10.1002/2015GB005310

Maher, N., Milinski, S., and Ludwig, R. (2021). Large ensemble climate model simulations: Introduction, overview, and future prospects for utilizing multiple types of large ensemble. *Earth System Dynamics*, 12(2), 401–418. doi: 10.5194/esd-12-401-2021

Mantua, N. J., Hare, S. R., Zhang, Y., Wallace, J. M., and Francis, R. C. (1997). A Pacific interdecadal climate oscillation with impacts on salmon production. *Bulletin of the*

American Meteorological Society, 78(6), 1069–1080. doi: 10.1175/1520-0477(1997)078%3C1069:APICOW%3E2.0.CO;2

Mauritsen, T., Bader, J., Becker, T., Behrens, J., Bittner, M., Brokopf, R., Brovkin, V., Claussen, M., Crueger, T., Esch, M., Fast, I., Fiedler, S., Fläschner, D., Gayler, V., Giorgetta, M., Goll, D. S., Haak, H., Hagemann, S., Hedemann, C., Hohenegger, C., Ilyina, T., Jahns, T., Jimenéz-de-la-Cuesta, D., Jungclaus, J., Kleinen, T., Kloster, S., Kracher, D., Kinne, S., Kleberg, D., Lasslop, G., Kornblueh, L., Marotzke, J., Matei, D., Meraner, K., Mikolajewicz, U., Modali, K., Möbis, B., Nyawira, S., Paulsen, H., Peters, K., Pincus, R., Pohlmann, H., Pongratz, J., Popp, M., Raddatz, J. R., Rast, S., Redler, R., Reick, C. H., Rohrschneider, T., Schemann, V., Schmidt, H., Schnur, R., Schulzweida, U., Six, K. D., Stein, L., Voigt, A., Vrese, P., Wieners, K., Wilkenskjeld, S., Winkler, A., and Roeckner, E. (2019). Developments in the MPI-M Earth System Model version 1.2 (MPI-ESM1.2) and Its Response to Increasing CO2. *Journal of Advances in Modeling Earth Systems*, 11(4), 998–1038. doi: 10.1029/2018MS001400

Mecking, S., Langdon, C., Feely, R. A., Sabine, C. L., Deutsch, C. A., and Min, D. H. (2008). Climate variability in the North Pacific thermocline diagnosed from oxygen measurements: An update based on the U.S. CLIVAR/CO2 Repeat Hydrography cruises. *Global Biogeochemical Cycles*, 22(3). doi: 10.1029/2007GB003101

Müller, W. A., Jungclaus, J. H., Mauritsen, T., Baehr, J., Bittner, M., Budich, R., Bunzel, F., Esch, M., Ghosh, R., Haak, H., Ilyina, T., Kleine, T., Kornblueh, L., Li, H., Modali, K., Notz, D., Pohlmann, H., Roeckner, E., Stemmler, I., Tian, J., and Marotzke, J. (2018). A Higher-resolution Version of the Max Planck Institute Earth System Model (MPI-ESM1.2-HR). *Journal of Advances in Modeling Earth Systems*, 10(7), 1383–

1413. doi: 10.1029/2017MS001217

Nakanowatari, T., Ohshima, K. I., and Wakatsuchi, M. (2007). Warming and oxygen decrease of intermediate water in the northwestern North Pacific, originating from the Sea of Okhotsk, 1955-2004. *Geophysical Research Letters*, 34(4), 10–13. doi: 10.1029/2006GL028243

Nishioka, J, Obata, H, Ogawa, H, and Yasuda, I. (2020). Subpolar marginal seas fuel the North Pacific through the intermediate water at the termination of the global ocean circulation. *Earth, Atmospheric, and Planetary Sciences*. 117 (23), 12665–12673, doi: 10.1073/pnas.200065811

Notz D., SIMIP Community (2020). Arctic Sea ice in CMIP6. *Geophysical Research Letters*. 47 (10), 1–11. doi: 10.1029/2019GL086749

Oka, E., Yamada, K., Sasano, D., Enyo, K., Nakano, T., and Ishii, M. (2019). Remotely Forced Decadal Physical and Biogeochemical Variability of North Pacific Subtropical Mode Water Over the Last 40 Years. *Geophysical Research Letters*, 46(3), 1555–1561. doi: 10.1029/2018GL081330

O'Neill, B. C., Tebaldi, C., van Vuuren, D. P., Eyring, V., Friedlingstein, P., Hurtt, G., Knutti, R., Kriegler, E., Lamarque, J. -F., Lowe, J., Meehl, G. A., Moss, R., Riahi, K., and Sanderson, B. M. (2016). The Scenario Model Intercomparison Project (ScenarioMIP) for CMIP6. *Geoscientific Model Development*, 9, 3461–3482. doi: 10.5194/gmd-9-3461-2016

Ono, T., Midorikawa, T., Watanabe, Y. W., Tadokoro, K., and Saino, T. (2001). Temporal increases of phosphate and apparent oxygen utilization in the subsurface waters of western subarctic Pacific from 1968 to 1998. *Geophysical Research Letters*, 28(17), 3285-3288. doi: 10.1029/2001GL012948

Osafune, S., and Yasuda, I. (2006). Bidecadal variability in the intermediate waters of the northwestern subarctic Pacific and the Okhotsk Sea in relation to 18.6-year period nodal tidal cycle. Journal of *Geophysical Reseach*, 111, C05007. doi: 10.1029/2005JC003277

Oschlies, A., Brandt, P., Stramma, L., and Schmidtko, S. (2018). Drivers and mechanisms of ocean deoxygenation. *Nature Geoscience*, 11(7), 467–473. doi: 10.1038/s41561-018-0152-2

Oschlies, A., Duteil, O., Getzlaff, J., Koeve, W., Landolfi, A., and Schmidtko, S. (2017). Patterns of deoxygenation: Sensitivity to natural and anthropogenic drivers. *Philosophical Transactions of the Royal Society A: Mathematical, Physical and Engineering Sciences*, 375(2102). doi: 10.1098/rsta.2016.0325

Pan, X, Achterberg, E. P., Sanders, R., Poulton, A. J., Oliver, K. I.C., and Robinson, C. (2014). Dissolved organic carbon and apparent oxygen utilization in the Atlantic Ocean. *Deep Sea Research Part I: Oceanographic Research Papers*, 85, 80–87. doi: 10.1016/j.dsr.2013.12.003

Pierce, S. D., Barth, J. A., Kipp Shearman, R., and Erofeev, A. Y. (2012). Declining oxygen in the northeast Pacific. *Journal of Physical Oceanography*, 42(3), 495–501. doi: 10.1175/JPO-D-11-0170.1

Plattner, G. K., Joos, F., and Stocker, T. F. (2002). Revision of the global carbon budget due to changing air-sea oxygen fluxes. *Global Biogeochemical Cycles*, 16(4), 43-1-43–12. doi: 10.1029/2001gb001746

Ross, T., du Preez, C., and Ianson, D. (2020). Rapid deep ocean deoxygenation and acidification threaten life on Northeast Pacific seamounts. *Global Change Biology*, 26(11), 6424–6444. doi: 10.1111/gcb.15307

Sasano, D., Takatani, Y., Kosugi, N., Nakano, T., Midorikawa, T., and Ishii, M. (2015). Multidecadal trends of oxygen and their controlling factors in the western North Pacific. *Global Biogeochemical Cycles*, 29(7), 935–956. doi: 10.1002/2014GB005065

Sasano, D., Takatani, Y., Kosugi, N., Nakano, T., Midorikawa, T., and Ishii, M. (2018). Decline and Bidecadal Oscillations of Dissolved Oxygen in the Oyashio Region and Their Propagation to the Western North Pacific. *Global Biogeochemical Cycles*, 32(6), 909–931. doi: 10.1029/2017GB005876

Schmidtko S., Stramma L., and Visbeck, M. (2017). Decline in global oceanic oxygen content during the past five decades. *Nature*, 542, 335–339. doi: 10.1038/nature21399

Séférian, R., Berthet, S., Yool, A., Palmiéri, J., Bopp, L., Tagliabue, A., Kwiatkowski, L., Aumont, O., Christian, J., Dunne, J., Gehlen, M., Ilyina, T., John, J. G., Li, H., Long, M. C., Luo, J. Y., Nakano, H., Romanou, A., Schwinger, J., Stock, C., Santana-Falcón, Y., Takano, Y., Tjiputra, J., Tsujino, H., Watanabe, M., Wu, T., Wu, F., and Yamamoto, A. (2020). Tracking Improvement in Simulated Marine Biogeochemistry Between CMIP5 and CMIP6. *Current Climate Change Reports*, 6(3), 95–119. doi: 10.1007/s40641-020-00160-0

Stramma, L., Oschlies, A., and Schmidtko, S. (2012). Mismatch between observed and modeled trends in dissolved upper-ocean oxygen over the last 50 yr. *Biogeosciences*, 9(10), 4045–4057. doi: 10.5194/bg-9-4045-2012

Stramma, L., Schmidtko, S., Bograd, S. J., Ono, T., Ross, T., Sasano, D., and Whitney, F. A. (2020). Trends and decadal oscillations of oxygen and nutrients at 50 to 300 m depth in the equatorial and North Pacific. *Biogeosciences*, 17(3), 813–831. doi:

10.5194/bg-17-813-2020

Swart, N. C., Cole, J. N. S., Kharin, V. v., Lazare, M., Scinocca, J. F., Gillett, N. P., Anstey, J., Arora, V., Christian, J. R., Hanna, S., Jiao, Y., Lee, W. G., Majaess, F., Saenko, O. A., Seiler, C., Seinen, C., Shao, A., Sigmond, M., Solheim, L., Salzen, K. v., Yang, D., and Winter, B. (2019). The Canadian Earth System Model version 5 (CanESM5.0.3). *Geoscientific Model Development*, 12(11), 4823–4873. doi: 10.5194/gmd-12-4823-2019

Takano, Y., Ito, T., and Deutsch, C. (2018). Projected Centennial Oxygen Trends and Their Attribution to Distinct Ocean Climate Forcings. *Global Biogeochemical Cycles*, 32(9), 1329–1349. doi: 10.1029/2018GB005939

Takatani, Y., Sasano, D., Nakano, T., Midorikawa, T., and Ishii, M. (2012). Decrease of dissolved oxygen after the mid-1980s in the western North Pacific subtropical gyre along the 137°E repeat section. *Global Biogeochemical Cycles*, 26(2), 1–14. doi: 10.1029/2011GB004227

Tatebe, H, Ogura, T, Nitta, T, Komuro, Y, Ogochi, K, Takemura, T, Sudo, K, Sekiguchi, M, Abe, M, Saito, F, Chikira, M, Watanabe, S, Mori, M, Hirota, N, Kawatani, Y, Mochizuki, T, Yoshimura, K, Takata, K, O'ishi, R, Yamazaki, D, Suzuki, T, Kurogi, M, Kataoka, T, Watanabe, M, and Kimoto, M. (2019). Description and basic evaluation of simulated mean state, internal variability, and climate sensitivity in MIROC6. *Geoscientific Model Development*, 12, 2727–2765. doi: 10.5194/gmd-12-2727-2019

Taylor, K. E., Stouffer, R. J., and Meehl, G. A. (2011). An Overview of CMIP5 and the Experiment Design, *Bulletin of the American Meteorological Society*, 93, 485–498. doi: 10.1175/BAMS-D-11-00094.1

Tjiputra, J. F., Schwinger, J., Bentsen, M., L. Morée, A., Gao, S., Bethke, I., Heinze, C., Goris, N., Gupta, A., He, Y. C., Olivié, D., Seland, O., and Schulz, M. (2020). Ocean biogeochemistry in the Norwegian Earth System Model version 2 (NorESM2). *Geoscientific Model Development*, 13(5), 2393–2431. doi: 10.5194/gmd-13-2393-2020

Townhill, B. L., Pinnegar, J. K., Righton, D. A., and Metcalfe, J. D. (2017). Fisheries, low oxygen and climate change: how much do we really know? *Journal of Fish Biology*, 90, 723–750. doi: 10.1111/jfb.13203

Whitney, F. A., Freeland, H. J., and Robert, M. (2007). Persistently declining oxygen levels in the interior waters of the eastern subarctic Pacific. *Progress in Oceanography*, 75(2), 179–199. doi: 10.1016/j.pocean.2007.08.007

Yasuda, I., Osafune, S., and Tatebe, H., (2006). Possible explanation linking 18.6-year period nodal tidal cycle with bi-decadal variations of ocean and climate in the North Pacific. *Geophysical Research Letters*, 33, L08606, doi: 10.1029/2005GL025237

Zhang, S., Hu, Y., and Liu, J. (2023). Inter-model spreads of the climatological mean Hadley circulation in AMIP/CMIP6 simulations. *Climate Dynamics*. doi: 10.1007/s00382-023-06813-8

Zheng, X. T., Xie, S. P., Lv, L. H., and Zhou, Z. Q. (2016). Intermodel uncertainty in ENSO amplitude change tied to Pacific Ocean warming pattern. *Journal of Climate*, 29(20), 7265–7279. doi: 10.1175/JCLI-D-16-0039.1

Ziehn, T., Chamberlain, M. A., Law, R. M., Lenton, A., Bodman, R. W., Dix, M., Stevens, L., Wang, Y. P., and Srbinovsky, J. (2020). The Australian Earth System Model: ACCESS-ESM1.5. *Journal of Southern Hemisphere Earth Systems Science*, 70(1), 193–214. doi: 10.1071/ES19035

Zweng, M. M, Reagan, J. R., Seidov, D., Boyer, T. P., Locarnini, R. A., Garcia, H. E., Mishonov, A. V., Baranova, O. K., Weathers, K. W., Paver, C. R., and Smolyar, I. V. (2019). World Ocean Atlas 2018, Volume 2: Salinity. A. Mishonov, Technical Editor, *NOAA Atlas NESDIS* 82, 50pp

Table and Figures

Table 1. Coupled Model Intercomparison Project (CMIP) models used in this study. The "Ensemble (hist)" column represents the ensemble members provided for each model in the historical experiment, totaling 204 ensembles. The "Ensemble (future)" column represents the ensemble members provided for each model in the scenario experiments (RCP8.5 for CMIP5 and ssp5-8.5 for CMIP6), totaling 111 ensembles. The "variables" column indicates which models provide dissolved oxygen (O), potential temperature (T), sea ice volume (I), and DOC (C) outputs.

Model	Layer/ horizontal grid number	Ensemble (hist)	Ensemble (future)	variables
CMIP5				
CESM1-BGC Gent et al. (2011)	60/384×320	r1i1p1	r1i1p1	O, T, I, C
GFDL-ESM2G Dunne et al. (2013)	63/210×360	r1i1p1	r1i1p1	O, T, I, C
GFDL-ESM2M Dunne et al. (2013)	50/200×360	r1i1p1	r1i1p1	O, T, I, C
HadGEM2-CC Collins et al. (2011)	40/216×360	r1 - r3i1p1	r1 - r3i1p1	O, T, I
HadGEM2-ES Collins et al. (2011)	40/216×360	r1 - r4i1p1	r1, r3, r4i1p1	O, T, I
IPSL-CM5A-LR Dufresne et al. (2013)	31/149×182	r1 - r6i1p1	r1 - r4i1p1	O, T, I, C
IPSL-CM5A-MR Dufresne et al. (2013)	31/149×182	r1 - r3i1p1	r1i1p1	O, T, I, C
IPSL-CM5B-LR Dufresne et al. (2013)	31/149×182	r1i1p1	r1i1p1	O, T, I, C
MPI-ESM-LR Giorgetta et al. (2013)	40/220×256	r1 - r3i1p1	r1 - r3i1p1	O, T, I, C
MPI-ESM-MR Giorgetta et al. (2013)	40/404×802	r1 - r3i1p1	r1i1p1	O, T, I, C
CMIP6				
ACCESS-ESM1-5 Ziehn et al. (2020)	50/300×360	r1 - r40i1p1f1	r1 - r40i1p1f1	O, T, I
CanESM5 Swart et al. (2019)	45/291×360	r1 - r25i1p1f1	r1 - r10i1p1f1	O, T
GFDL-ESM4 Dunne et al. (2020)	35/180×360	r1i1p1f1		O, T, I, C
IPSL-CM6A-LR Boucher et al. (2020)	75/332×362	r1 - r33i1p1f1	r1 - r4, r6, r14, r33i1p1f1	O, T, I, C
MIROC-ES2L Hajima et al. (2020)	52/200×360	r1 - r30i1p1f2	r1i1p1f2	O, T, I
MPI-ESM1-2-HR Müller et al. (2018)	40/404×802	r1 - r10i1p1f1	r1, r2i1p1f1	O, T, I, C
MPI-ESM1-2-LR Mauritsen et al. (2019)	40/220×256	r1 - r30i1p1f1	r1 - r30i1p1f1	O, T, I, C
MPI-ESM-1-2-HAM Mauritsen et al. (2019)	40/220×256	r1 - r3i1p1f1		O, T, I, C
NorESM2-LM Tjiputra et al. (2020)	53/385×360	r1 - r3i1p1f1	r1i1p1f1	O, T, I, C
NorESM2-MM Tjiputra et al. (2020)	53/385×360	r1 - r3i1p1f1	r1i1p1f1	O, T, I, C

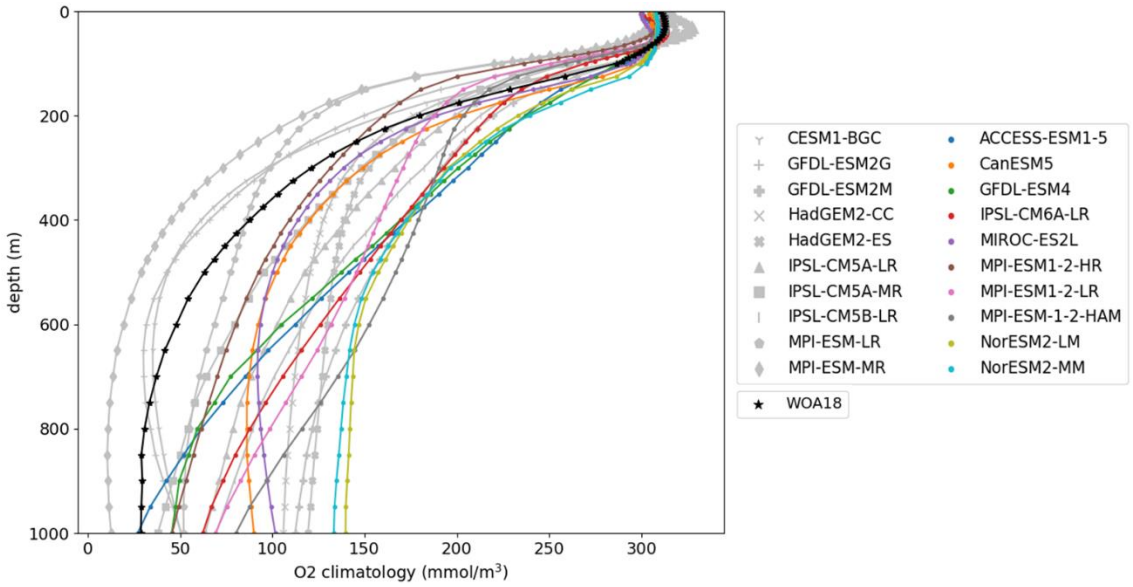

Figure 1. Vertical profile of regionally averaged O2 climatology in the subarctic region (40° to 65°N). Gray symbols represent the CMIP5 models and colored symbols represent the CMIP6 models. The black line shows the climatology based on the World Ocean Atlas 2018 (WOA18).

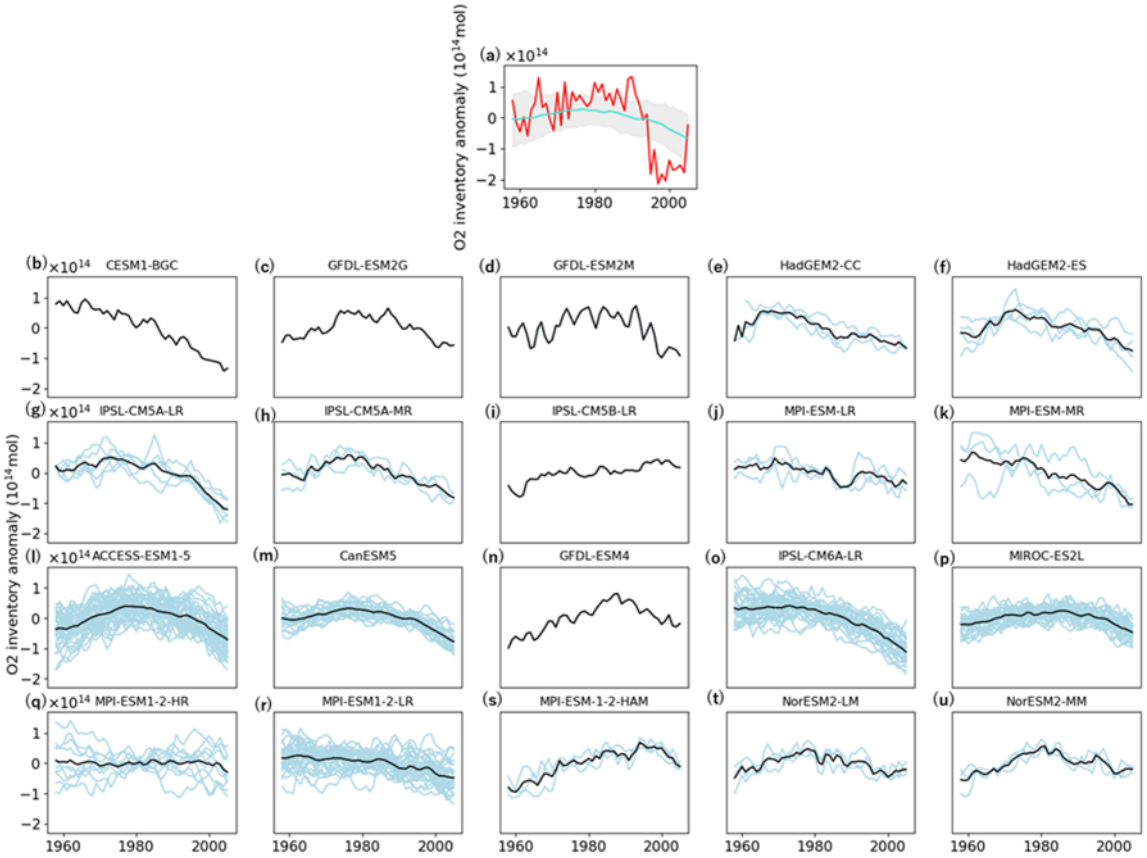

Figure 2. Anomalies in the O2 inventory from the surface to depths of 1000 m in the North Pacific from 1958 to 2005. In panel (a), the red and cyan lines indicate observed and MMEM inventories, respectively, whereas the shaded area indicates the range between the 95 and 5 percentiles among model ensembles for each year. In panel (b) to (u), the light blue lines represent the ensemble members, respectively and the black line is the ensemble mean.

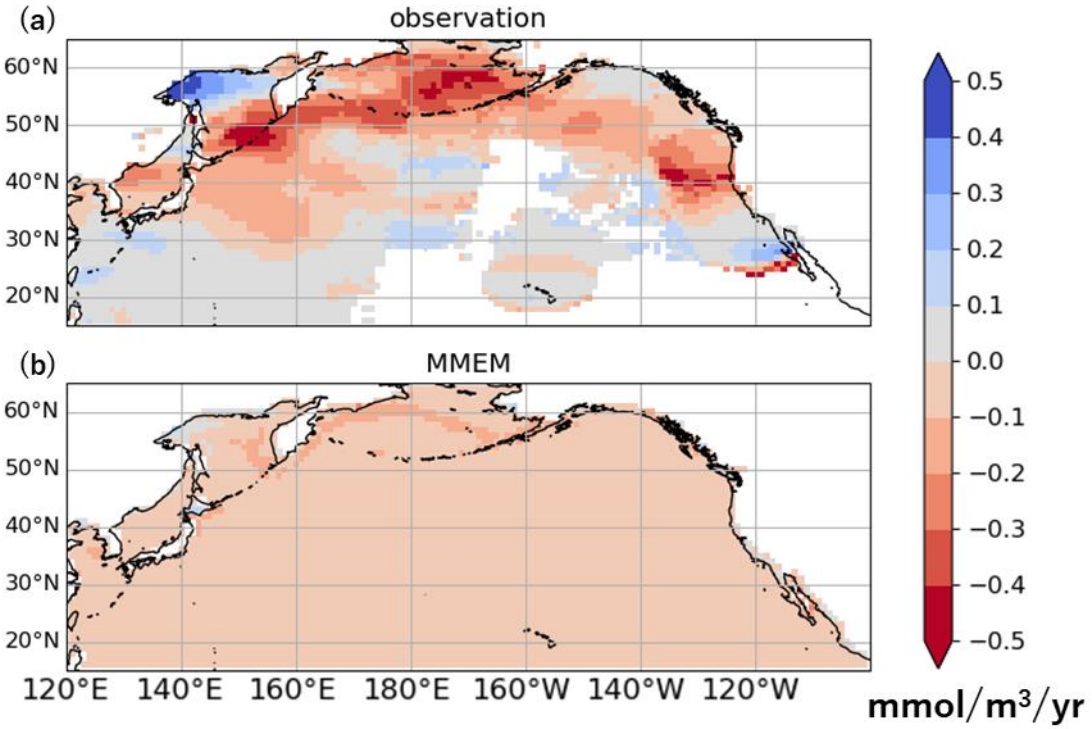

Figure 3. Vertical averages of O2 concentration trend from 1958 to 2005 in (a) observations, and (b) MMEM.

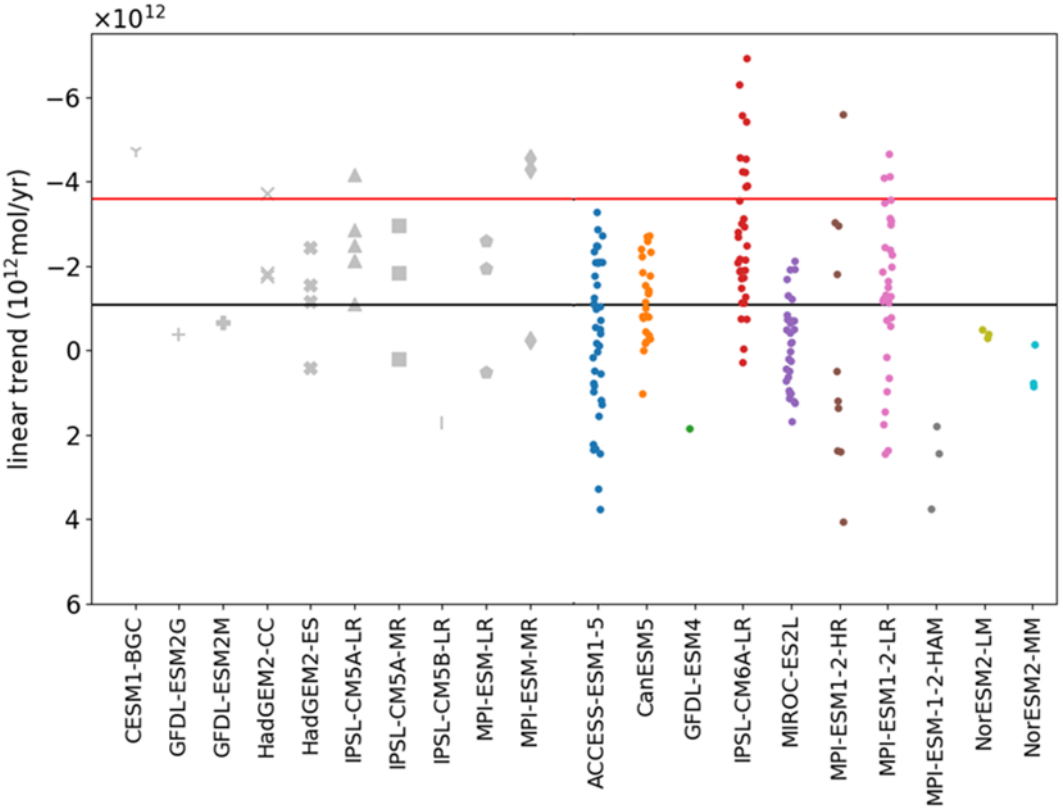

Figure 4. Trends of O2 inventory anomalies from 1958 to 2005 in the North Pacific from the surface to depths of 1000 m, with negative trends represented by upward bars. The red line shows the observational trend, and the black line shows the MMEM trend. Gray symbols represent the CMIP5 models and colored symbols represent the CMIP6 models.

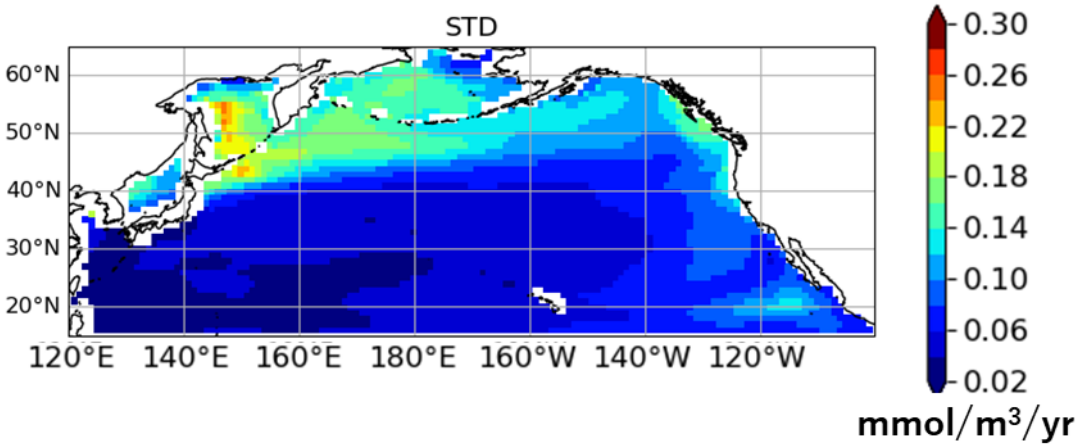

Figure 5. Standard deviation of the vertical averages of O2 concentration trend in 1958–2005 of the all model ensemble members.

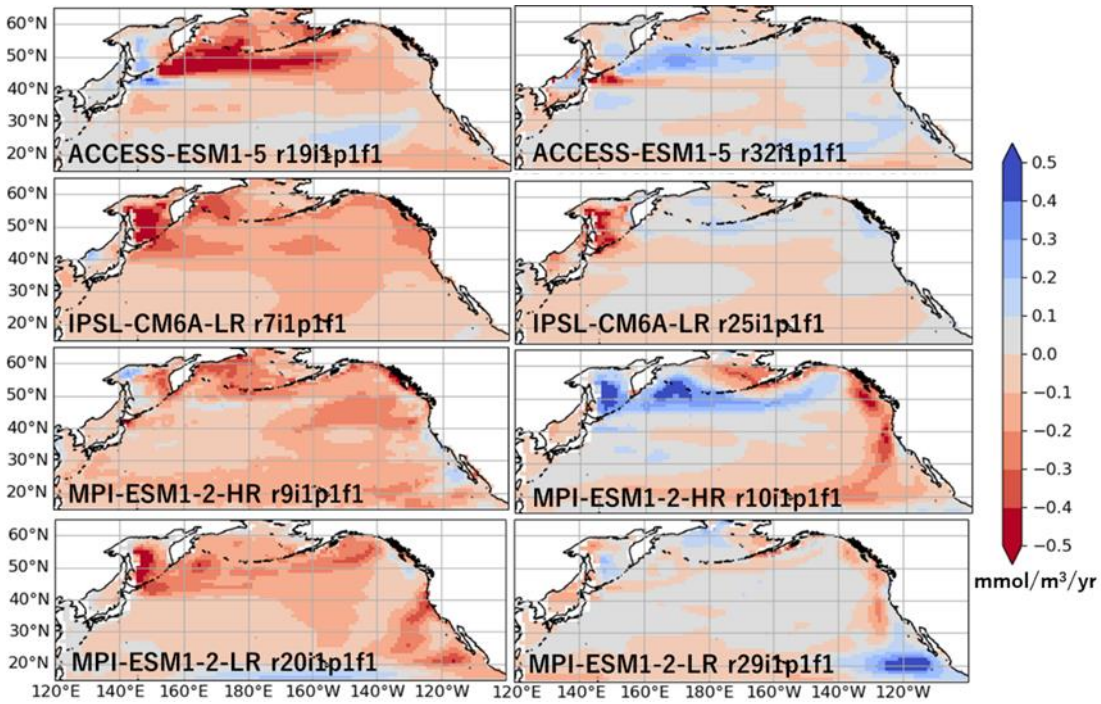

Figure 6. Vertical averages of O2 concentration trends from 1958 to 2005 in the top four models known for their large variability in O2 inventory trend (as shown in Figure 4). The left panels are the ensemble members characterized by the largest negative O2 inventory trend, while the right panels exhibit the ensemble member with the largest positive O2 inventory trend.

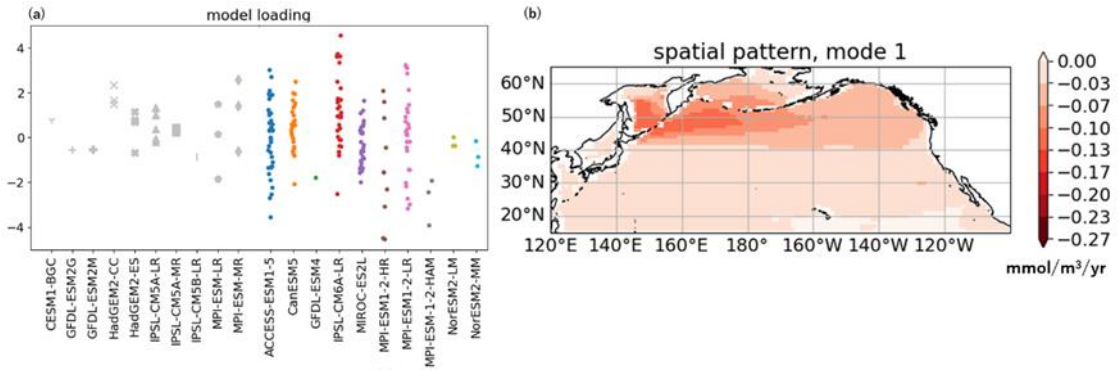

Figure 7. (a) Loading of the first EOF mode of the vertical averaged O2 concentration trend from 1958 to 2005 in model ensembles, (b) spatial distribution of the first mode. The color bar in (b) shows a different range from the color bars in Figures 3 and 6. In (a), symbols are the same as Figure 4.

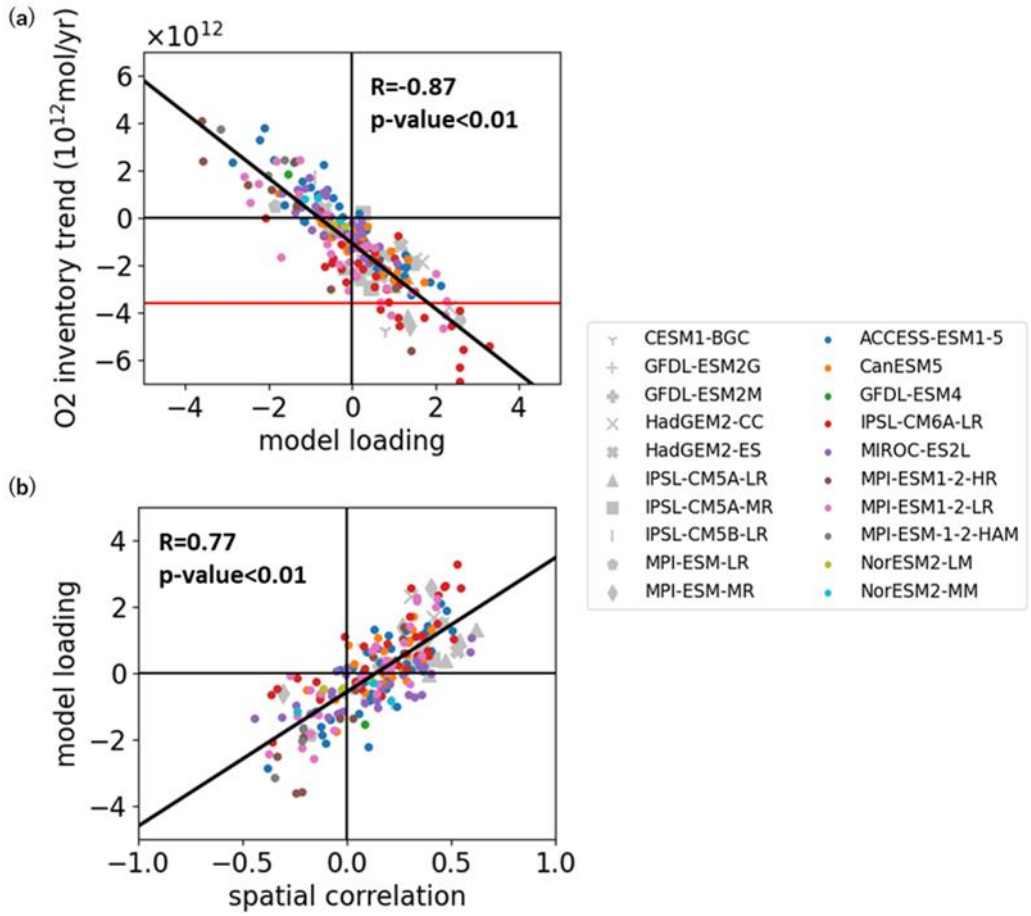

Figure 8. Scatter plots of the model loadings of the first EOF mode of the spatially distributed O2 trend and (a) the O2 inventory trend and (b) spatial correlation between the observation and each model ensemble member. The red line shows the observational trend. Gray symbols represent the CMIP5 models and colored symbols represent the CMIP6 models. Symbols are the same as Figures 4 and 7a.

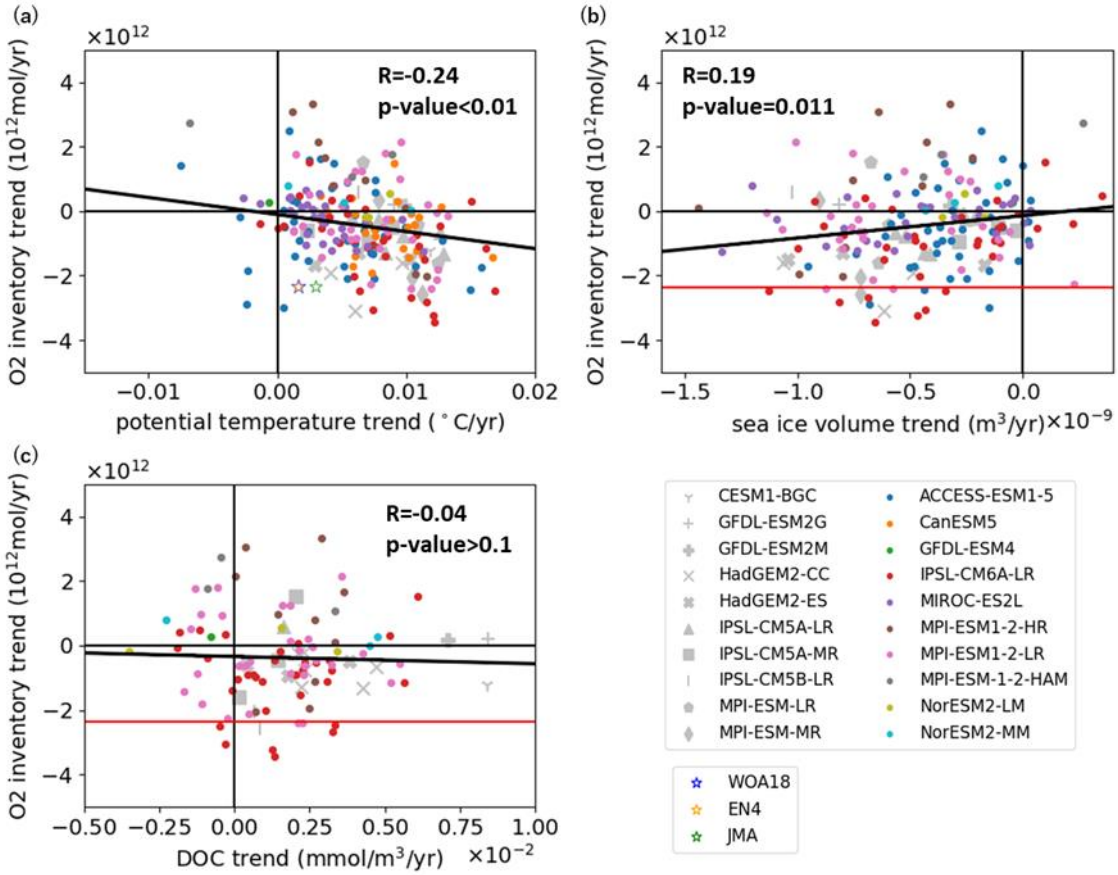

Figure 9. Scatter plots of the O2 inventory trend in the subarctic North Pacific and (a) potential temperature trend, (b) sea ice volume trend, and (c) DOC trend averaged in the subarctic North Pacific (40° to 65°N). Symbols are the same as Figure 8. Star symbols in (a) show the trends of the observations. The red line in (b) and (c) shows the observational trend.

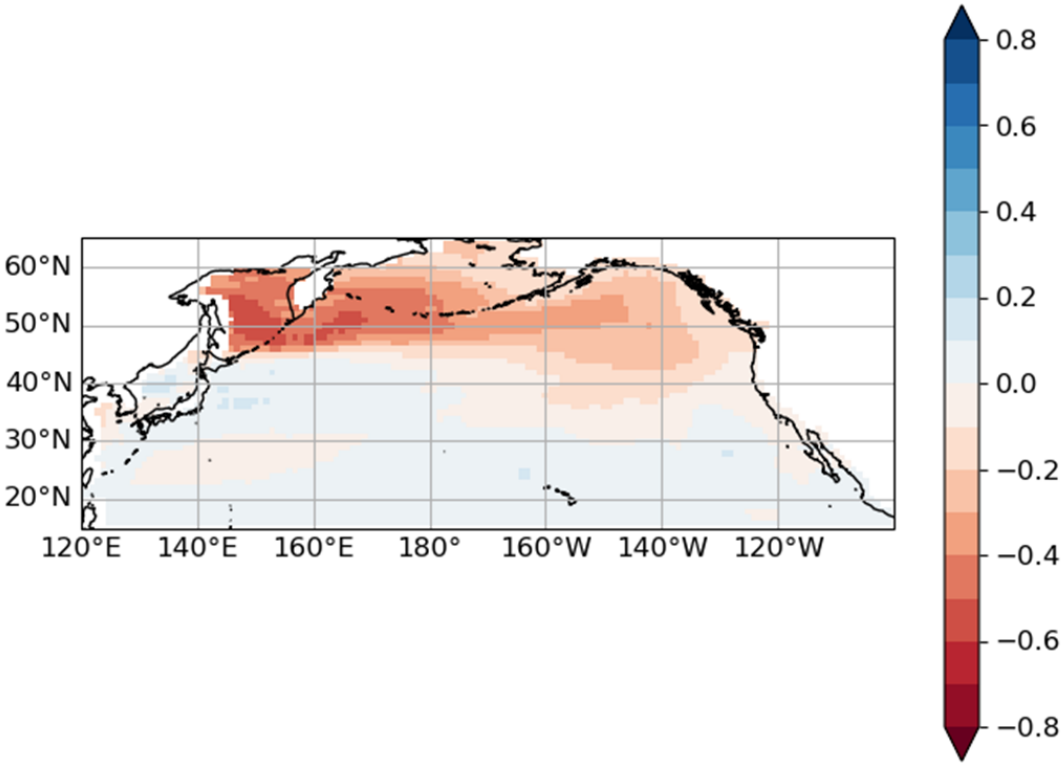

Figure 10. Correlation map between O2 inventory trend in the North Pacific and vertical averaged potential temperature among the model ensemble members.

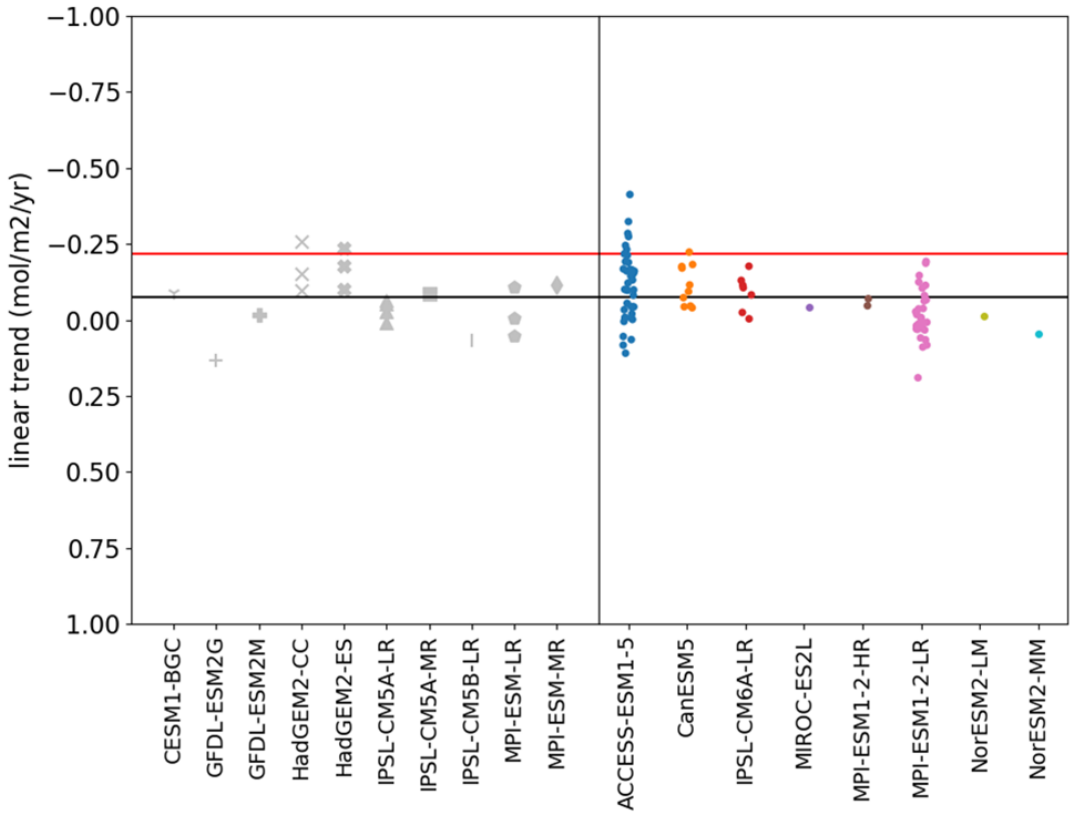

Figure 11. The trend of vertically integrated O2 concentration at Station P. The red line shows the observational trend, and the black line shows the MMEM trend. Symbols are the same as Figure 4.

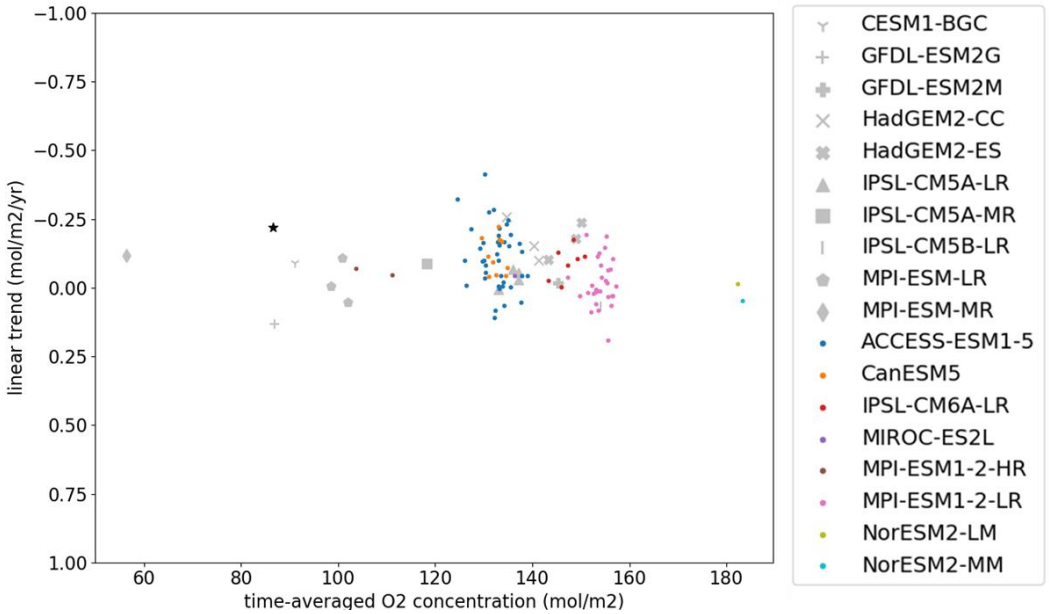

Figure 12. The scatter plot of the trend of vertically integrated O2 concentration against the time-averaged vertically integrated O2 concentration at Station P. Symbols are the same as Figure 4. Star symbol shows the observation.

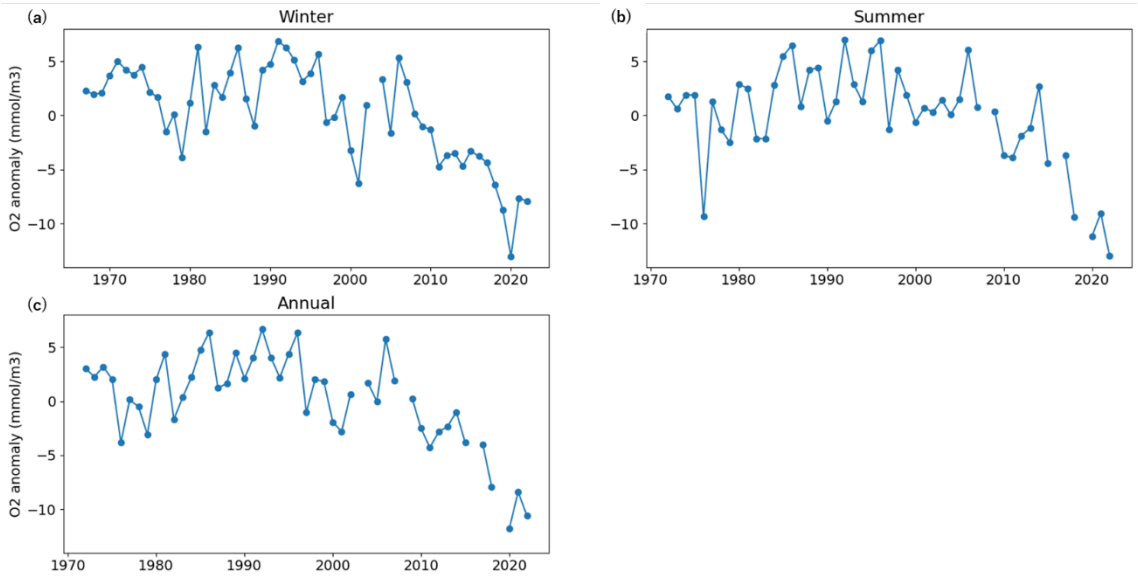

Figure 13. Area-averaged O2 concentration anomalies at depths from the surface to 1000 m between 15°N and 34°N of the 137°E line. (a) Winter data is from 1967 to 2022, (b) summer data is from 1972 to 2022, and therefore, the annual average (c) is calculated from 1972 to 2022, when both winter and summer data are available. The anomalies for all seasons are based on the average value from 1972 to 2022.

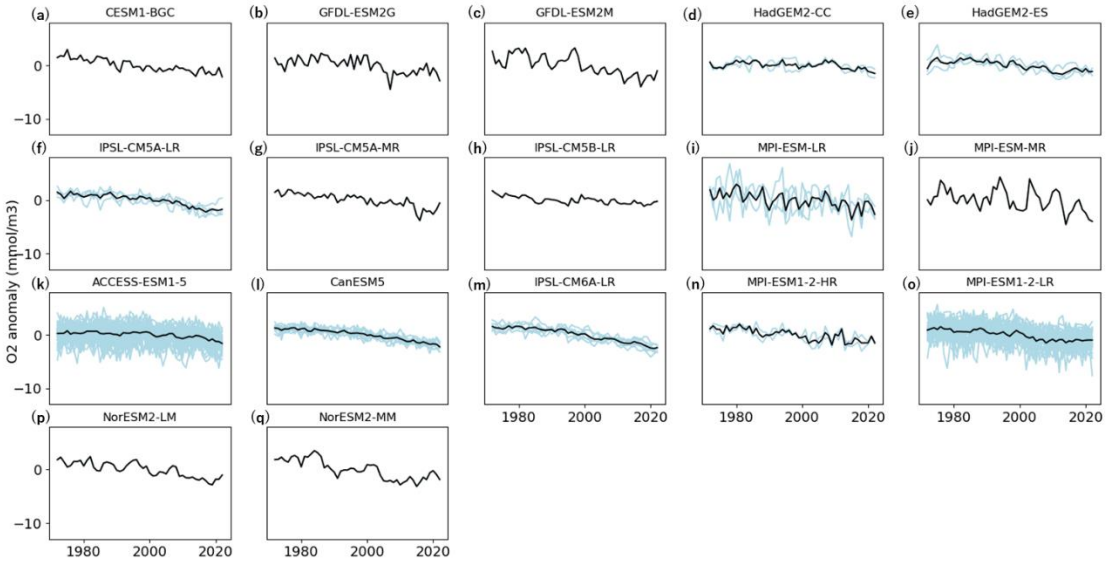

Figure 14. Area-averaged O2 concentration anomalies at depths from the surface to 1000 m between 15°N and 34°N of the 137°E line. The light blue lines represent the ensemble members, respectively and the black line is the ensemble mean.

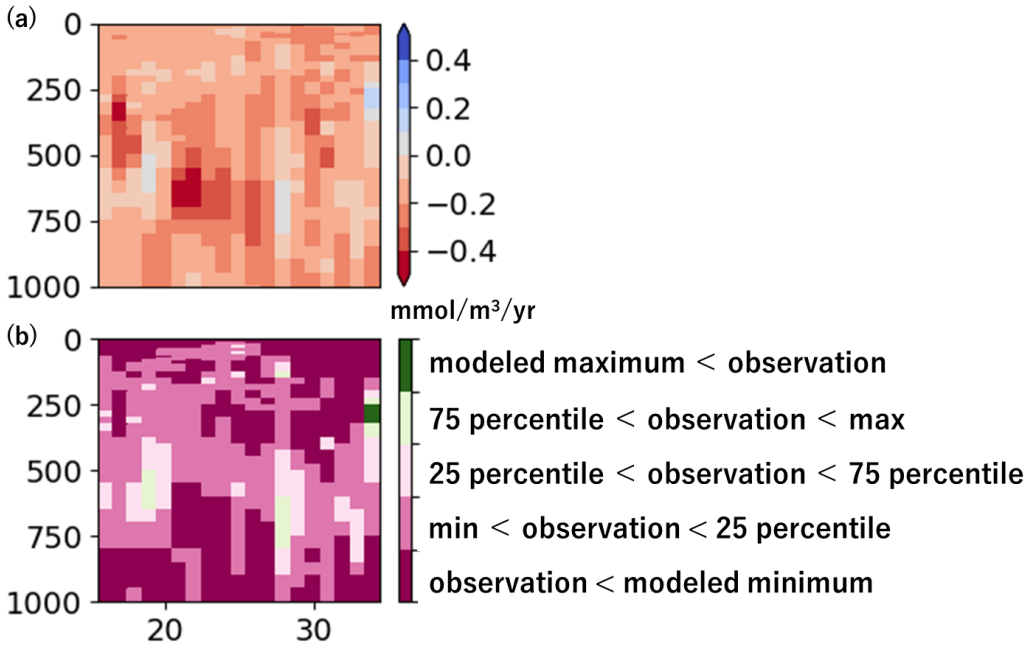

Figure 15. (a) Observed annual O2 concentration trend from 1972 to 2022 of the 137°E line, and (b) a cross-sectional figure showing the position of the observed trends within the range of model trend variations for each grid. The vertical axis represents isobath depth (m) and the horizontal axis represents latitude from 15° to 34°N.

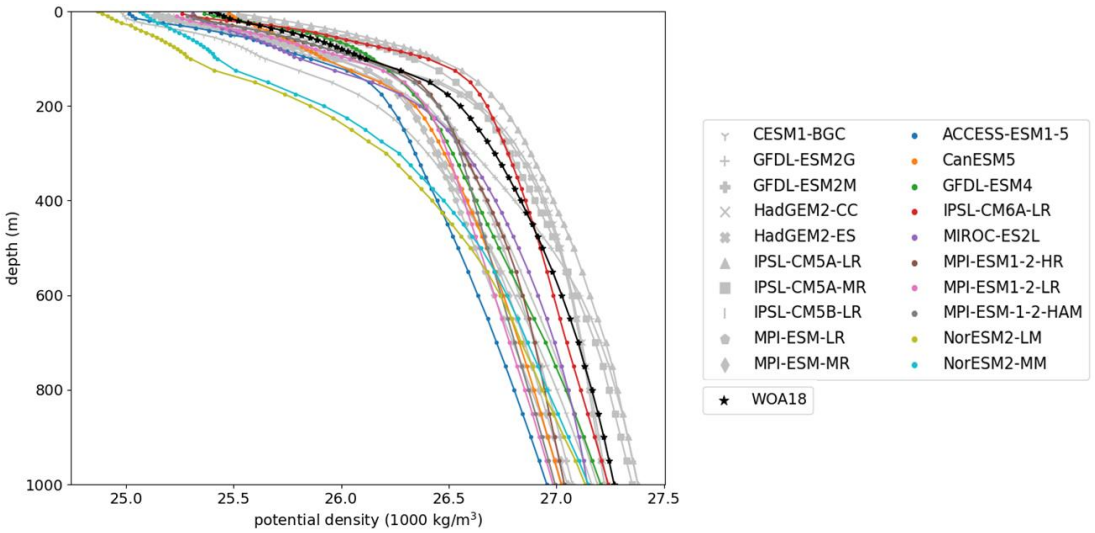

Figure 16. Vertical profile of regionally averaged potential density in the subarctic region (40° to 65°N). Symbols are the same as Figure 1.